Single cell multi-omics analysis of chronic myeloid leukemia links cellular heterogeneity to therapy response

Rebecca Warfvinge[1], Linda Geironson Ulfsson[1], Parashar Dhapola[1], Fatemeh Safi[1], Mikael N.E. Sommarin[1], Shamit Soneji[1], Henrik Hjorth-Hansen[2,3], Satu Mustjoki[4,5,6], Johan Richter[7,8], Ram Krishna Thakur*[1], Göran Karlsson*[#1]

* These authors contributed equally; [#] Lead contact

[1] Division of Molecular Hematology, Lund Stem Cell Center, Lund University, Sweden

[2] Department of Hematology, St Olavs Hospital, Trondheim, Norway

[3] Department of Cancer Research and Molecular Medicine, Norwegian University of Science and Technology (NTNU), Trondheim, Norway

[4] Translational Immunology Research Program and Department of Clinical Chemistry and Hematology, University of Helsinki, Helsinki, Finland

[5] Hematology Research Unit Helsinki, Helsinki University Hospital Comprehensive Cancer Center, Helsinki, Finland

[6] iCAN Digital Precision Cancer Medicine Flagship, Helsinki, Finland

[7] Division of Molecular Medicine and Gene Therapy, Lund Stem Cell Center, Lund University, Sweden

[8] Department of Hematology, Oncology and Radiation Physics, Skåne University Hospital, Lund, Sweden

Correspondence: ram_krishna.thakur@med.lu.se

Correspondence and lead contact: goran.karlsson@med.lu.se

Abstract

The advent of tyrosine kinase inhibitors (TKIs) as treatment of chronic myeloid leukemia (CML) is a paradigm in molecularly targeted cancer therapy. Nonetheless, TKI insensitive leukemia stem cells (LSCs) persist in most patients even after years of treatment. The sustained presence, heterogeneity and evolvability of LSCs are imperative for disease progression as well as recurrence during treatment-free remission (TFR). However, dynamic changes among LSC sub-populations upon TKI therapy impede their measurement and targeting. Here, we used cellular indexing of transcriptomes and epitopes by sequencing (CITE-seq) to generate high-resolution single cell multiomics maps from CML patients at diagnosis, retrospectively stratified by BCR::ABL1^{IS} (%) following 12 months of TKI therapy as per European LeukemiaNet (ELN) recommendations. Simultaneous measurement of global gene expression profiles together with >40 surface markers from the same cells revealed that each patient harbored a unique composition of stem and progenitor cells at diagnosis demonstrating that cellular heterogeneity is a hallmark of CML. The patients with treatment failure after 12 months of therapy had markedly higher abundance of molecularly defined primitive cells at diagnosis compared to the optimal responders. Furthermore, deconvolution of an independent dataset of CML patient-derived bulk transcriptomes (n=59) into constituent cell populations showed that the proportion of primitive cells versus lineage primed sub-populations significantly connected with the TKI-treatment outcome. The multiomic feature landscape enabled visualization of the primitive fraction as a heterogenous mixture of molecularly distinct Lin$^-$CD34$^+$CD38$^{-/low}$ BCR::ABL1$^+$ LSCs and BCR::ABL1$^-$ hematopoietic stem cells (HSCs) in variable ratio across patients and guided their prospective isolation by a combination of CD26 and CD35 cell surface markers. We for the first time show that BCR::ABL1$^+$ LSCs and BCR::ABL1$^-$ HSCs can be distinctly separated as CD26$^+$CD35$^-$ and CD26$^-$CD35$^+$ respectively. In addition, we found the relative proportion of CD26$^-$CD35$^+$ HSCs to be higher in optimal responders when compared to treatment failures, at diagnosis as well as following 3 months of TKI therapy, and that the LSC/HSC ratio was increased in patients with prospective treatment failure. Collectively, the patient-specific cellular heterogeneity multiomics maps build a framework towards understanding therapy response and adapting treatment by devising strategies that either extinguish TKI-insensitive LSCs or engage the immune effectors to suppress the residual leukemogenic cells.

Introduction

The persistence, burden and evolvability of leukemic stem cells (LSCs) during therapy provide common threads to address the major challenges remaining in chronic myeloid leukemia (CML) (Cortes et al., 2021; Michor et al., 2005). For example, acquisition of the BCR::ABL1 kinase domain (KD), and additional somatic mutations within LSCs could either necessitate a switch to another tyrosine kinase inhibitor (TKI) or precipitate a blast crisis (Bolton-Gillespie et al., 2013; Giustacchini et al., 2017; Nieborowska-Skorska et al., 2012; O'Hare et al., 2007; Sorel et al., 2004). Moreover, even in the absence of KD mutations, the LSC burden at diagnosis is linked to cytogenetic and molecular response in chronic phase (Khorashad et al., 2006; Mustjoki et al., 2013), and their presence is associated with recurrence during treatment-free remission (TFR)(Pagani et al., 2020), thus compelling life-long treatment in the majority of patients.

The de facto standard for disease monitoring, BCR::ABL1 transcript/gDNA quantification using qPCR, Sanger and/or Next Generation Sequencing (NGS), however, predictably only captures cells positive for BCR::ABL1 expression and translocation and does not inform the number and identity of fully leukemogenic cells (Radich et al., 2019). This is pertinent given that a combination of cell sorting and BCR::ABL1 quantification suggested that the presence of BCR::ABL1 signal in the stem cell compartment rather than the lymphocytes correlates with TFR loss (Kinstrie et al., 2020; Pagani et al., 2020). Using hematopoietic stem cell (HSC) specific markers however, is confounded by the observations that in remission, patients in chronic phase restore Philadelphia chromosome-negative (Ph^-) hematopoiesis (Bergamaschi et al., 1994; Carella et al., 1993; Claxton et al., 1992; Coulombel et al., 1983; Deininger, 2003), implying the co-existence of $BCR::ABL1^-$ HSCs and $BCR::ABL1^+$ LSCs. However, because their proportion varies across individuals and treatment stages (Mustjoki et al., 2013), and both LSCs and HSCs reside within similar immunophenotypic compartment ($Lin^-CD34^+CD38^{-/low}$) (Eisterer et al., 2005; Petzer et al., 1996), discrimination between these populations – and thereby reliably estimating LSCs – remains difficult. As a result, understanding CML LSC identity, heterogeneity, and vulnerability to TKI therapy remain outstanding challenges in CML.

We recently implemented BCR::ABL1 targeted single-cell RT-qPCR in combination with index sorting for surface markers to dissect the LSC compartment at diagnosis and following 3 months of TKI-therapy (Warfvinge et al., 2017). This demonstrated that at diagnosis, $Lin^-CD34^+CD38^{-/low}$ $BCR::ABL1^+$ cells could be divided into seven molecularly distinct subpopulations, each reflecting unique lineage and cell state signatures. Importantly, the proportions of $BCR::ABL1^+$ LSC subpopulations changed dynamically upon therapy and only a few surface markers efficiently discriminated between $BCR::ABL1^+$ vs. $BCR::ABL1^-$ cells. Of these, despite being generally reduced in $BCR::ABL1^+$ cells upon therapy, CD26 was more frequently detected on the subpopulation most persistent during TKI treatment. The substantial treatment-induced changes observed within the stem cell population suggested that $BCR::ABL1^+$ LSCs

are themselves heterogeneous in terms of sensitivity to TKIs allowing us to define BCR::ABL1^{+}Lin^{-}CD34^{+}CD38$^{-/low}$CD45RA^{-}cKIT^{-}CD26^{+} as the most TKI-insensitive cells. Apart from being detected at diagnosis, these cells are strikingly enriched after TKI therapy (Warfvinge et al., 2017), a finding since confirmed in a transgenic mouse model (Shah et al., 2023), and in clinical observations documenting long-term persistence of CD26^{+} cells in CML patients (Pacelli et al., 2023). Together, these findings argue that functional heterogeneity within LSCs cannot be predicted solely by surface markers but is intimately linked to their cell state and gene expression signature, thereby motivating a strategy to simultaneously capture their lineage potency/affiliation, BCR::ABL1 status, and molecular program in addition to the surface markers.

Although recent single cell omics studies have begun to explore the cellular landscape in CML (Giustacchini et al., 2017; Krishnan et al., 2023; Patel et al., 2022; Zhang et al., 2020), these have largely been limited to measuring single modalities at a time, and thus, multiomic investigation of BCR::ABL1^{+} LSCs and BCR::ABL1^{-} stem cells from the same patient are currently lacking. Therefore, we used cellular indexing of transcriptomes and epitopes by sequencing (CITE-seq) (Stoeckius et al., 2017) to quantify the global gene expression program, and highly multiplexed cell-surface protein profile simultaneously within the same cells from nine CML patients. The single cell multiomics maps enabled us to visualize the cellular heterogeneity of each patient by delineating the abundance of molecularly defined leukemic stem versus lineage progenitors, and link cell composition at diagnosis to TKI therapy response. Moreover, the maps highlighted the co-existence of molecularly distinct BCR::ABL1^{+} vs. BCR::ABL1^{-} stem cells, guiding their prospective isolation by novel combinations of CD26 and CD35 markers, dissection of imbued molecular programs, division kinetics and changes in heterogeneity following TKI therapy.

Results

Single-cell multiomic CITE-seq analysis defines the heterogeneity of CML stem cell fractions

To characterize the multimodal heterogeneity within the Lin^{-}CD34^{+} and Lin^{-}CD34^{+}CD38$^{-/low}$ CML bone marrow (BM) compartment at diagnosis and estimate how the heterogeneity contributes to therapy response, we applied CITE-seq on nine patient retrospectively stratified according to molecular response following 12 months of treatment. To allow for accurate specification of LSPC heterogeneity without confounding effects generated from cell-type-irrelevant transcriptional signals related to BCR-ABL transformation per se, or inter patient variability due to batch effects, we used Scarf projection (Dhapola et al., 2022) to map each individual CML cell to a Lin^{-}CD34^{+} healthy bone marrow reference with a predefined heterogeneity. Each CML cell was then annotated by label transfer according to the annotation of the reference cells with highest molecular similarity (Fig. 1A).

The CITE-seq analysis combines single cell RNA-seq with simultaneous staining for a panel of >40 antibodies conjugated to uniquely barcoded oligonucleotides (henceforth Antibody derived tags, ADTs) aimed to cover the spectrum of normal hematopoietic stem ($CD34^+CD38^{-/low}$ fraction) and lineage progenitors ($CD34^+$ enriched fraction, HSPCs) as well as surface markers reported to enrich for CML stem cells (Herrmann et al., 2014; Jaras et al., 2010; Kinstrie et al., 2020; Landberg et al., 2018; Sadovnik et al., 2016; Warfvinge et al., 2017). Upon sequencing, the scRNA-seq and ADT-seq libraries provide concurrent readout of gene expression and abundance of surface proteins respectively. This multiomic approach surpasses scRNA-seq in cellular subtype characterization and is not constrained by the conundrum of spectral overlap of fluorophores in FACS (Stoeckius et al., 2017), and availability of metal isotopes in mass cytometry as noted previously (Gullaksen et al., 2019). Our sample set of nine CML patients are from various clinical studies with attendant information on BCR::ABL1 transcript level as per International Scale (IS %) available after 12 months of TKI therapy. These were retrospectively classified as optimal, treatment failures, and warning cases in accordance with the guidelines from European LeukemiaNet (ELN) (Hochhaus et al., 2020) (Supp. Table 1).

To build a normal reference, we used our recently described CITE-seq profiles of Lin^-CD34^+ cells from normal BM from two age-matched healthy donors (henceforth, nBM) (Sommarin et al., 2021). The normal reference of 4696 Lin^-CD34^+ cells was visualized in a Uniform Manifold Approximation and Projection (UMAP, Fig. 1B). Although single cell omics datasets generate expression values for several thousand genes (dimensions), not all are equally informative. UMAP is a non-linear algorithm for dimensionality reduction and preserves the global data structure and enables visualization of the dataset in two dimensions. The nBM cells were subsequently clustered and annotated based on marker genes as well as information from antibody derived tags (ADTs) against surface markers (Fig. 1C-D, Supp. Table 4). We identified eleven cell clusters consisting of primitive cells, lineage progenitors and cycling cells in the UMAP, with near to equal distribution across the two nBM samples (Supp. Fig. 1). The primitive cluster was marked by expression of stem-like gene expression e.g., CRHBP, HLF as well as a $CD90^+CD38^{-/low}$ surface profile. Closest to the primitive cluster were MPP1 and 2 without frank manifestation of lineage specific markers. The MPP1 cluster, in turn, was connected to the clusters with gain of myeloid-like, and lymphoid-like gene expression programs. This included myelo/lymphoid (My/Ly), myeloid (My: MPO, CD33), and lymphoid/dendritic/monocyte (Ly/pDc/mono) clusters (Ly86, CD135). The MPP2 cluster, in comparison, was connected to the megakaryocyte and erythroid lineage progenitors such as megakaryocyte-erythroid (MEP), megakaryocyte (MkP: ITGA2B, CD41), erythroid progenitors (ErP: HBA1, CD71, CD105) and basophil/mast cell clusters (Baso/mc: HDC, MS4A2-3, ITGB7).

Following CITE-seq of 14,274 Lin^-CD34^+ cells from nine CML patients, the cells were projected onto the nBM reference and annotated by label-transfer. Subsequently, we generated UMAPs for each patient and color-coded cells according to the transferred

labels enabling us to visualize and highlight cellular heterogeneity on an individual basis (Fig. 2A, Supp. Fig. 2A). A comparison of abundance of clusters showed that CML patients, in general, were enriched for basophil/mast cell, MEP, MkP clusters and depleted for primitive, MPP1, 2, and ly/pDC/Mono clusters (Fig. 2B). Inspection of profiles per patient showed that while most of the clusters were consistently enriched or depleted, ErP progenitors and cycling cells showed highly individual patterns (Supp. Fig. 2B). Furthermore, visual inspection of the individual UMAPs revealed an intriguing and distinct separation of cells within the primitive cluster in most of the patients (Fig. 2A). Taken together, CITE-seq and label transfer through nBM reference cell projection could successfully define the molecular heterogeneity within the Lin^- $CD34^+$ LSPC at diagnosis and revealed an average increase in abundance of MEP, MkP, and basophil/mast cells as compared to nBM.

Identification of gene signatures unique to CML cells and shared across CML stem and progenitor populations

The identification of nBM and CML primitive populations and lineage progenitors prompted us to systematically compare pair-wise gene expression differences between all eleven clusters in CML and their nBM counterparts (Fig. 2C, Supp. Table 5). For each pair-wise comparison, we highlighted only the genes that were differentially expressed between the pair but not shared with any other cluster thereby defining strict cluster-specific changes. Although this revealed unique changes across all cluster pairs, the most striking changes were seen between primitive clusters from CML versus nBM with 384 differentially expressed genes. Moreover, erythroid progenitors also displayed large changes followed by ly/pDC/mono and ErP progenitors.

In contrast, when considering genes differentially expressed in CML relative to nBM, and crucially shared among all the cluster comparisons, we identified a set of 71 genes that comprised a pan-cml signature. This approach is preferrable to a 'bulk' comparison of all CML $CD34^+$ cells lumped together versus nBM cells, where the most numerically abundant cluster, and the most highly expressed genes therein, are likely to contribute disproportionately (Fig. 2D). Of the 71 genes, 50 genes were found to be consistently up-regulated in CML stem and progenitors. Notably, the individual genes from this set were expressed at varying levels in individual clusters (Supp. Fig. 3A, Supp. Table 6), reflecting a heterogenous origin of the CML signature. This included a constellation of genes such as surface markers, CD81 (Quagliano et al., 2020), nucleoside diphosphate kinase with transcriptional regulatory activity, NME2 (Kar et al., 2012; Thakur et al., 2009; Thakur et al., 2014; Thakur et al., 2011; Tschiedel et al., 2012; Tschiedel et al., 2008; Yadav et al., 2014) previously implicated in CML, genes of histone family, and components of SWI/SNF chromatin remodeling complex, BRD7 (Kaeser et al., 2008), as well as genes of histone methyltransferase family, KMT3A and 5A (Husmann & Gozani, 2019). The analysis also identified 21 genes specifically and consistently upregulated in all clusters across nBM versus CML, and among others included DPY30 gene implicated in maintenance of adult HSCs (Yang et al., 2016).

Progenitor heterogeneity at diagnosis is linked to TKI therapy outcome

To assess how cellular heterogeneity within the $Lin^{-}CD34^{+}$ compartment at diagnosis is related to therapy response, the patients were stratified according to $BCR::ABL1^{IS}$ (%) following 12 months of TKI therapy as per ELN recommendations (Supp. Table 1). The stem and progenitor heterogeneity at diagnosis was then evaluated relative to the treatment outcome by assessing cell composition of the individual CML patients 1-9 classified as optimal (CML1-4), warning (CML 5-7), and treatment failure (CML 8-9).

By enumerating the proportion of molecularly defined clusters of individual patients, we found that all clusters from the normal bone marrow reference samples were represented in each patient. However, there was remarkable heterogeneity between patients in terms of relative abundance of constituent clusters (Fig. 3A, Supp. Fig. 2B). Importantly, this inter-patient heterogeneity followed patterns connected to therapy outcome. A focused comparison between optimal responders (CML 1-4) and treatment failure cases (CML 8-9) showed distinctive enrichment of specific cell clusters (Fig. 3B), where failure cases displayed a higher abundance of the molecularly defined primitive cluster, multipotent progenitors 1 and 2, and myelo-lymphoid (My/Ly) and Ly/pDC/monocyte clusters at diagnosis. In contrast, the optimal responders had a higher burden of megakaryocyte-erythroid progenitors (MEP), megakaryocyte progenitors (MkP), Erythroid progenitor (ErP), Baso/mc and cycling clusters at diagnosis. Among others, the most conspicuous changes between optimal responders and treatment failures were observed in the primitive cluster (~4 fold higher in failures), and Meg-erythroid progenitors (MEP) and erythroid cluster (~3 fold higher in optimal). The warning cases (CML 5-7) also showed heterogeneity in terms of cell composition (Fig. 3A); for instance, while CML 5 had a relatively higher content of primitive cells akin to treatment failures, CML 6 and 7 had a profile resembling optimal responders. Thus, these observations indicate that the prospective treatment outcome is reflected by the composition of stem and progenitor cell types at diagnosis.

Large scale deconvolution of independent dataset shows cell composition is linked to cytogenetic response to TKI therapy

To further assess whether the hematopoietic stem and progenitor composition of CML patients at diagnosis is connected to their therapy response, we utilized an independent publicly available bulk gene expression dataset from CML patients with known therapy response (n=59) (McWeeney et al., 2010). This was done with an aim to computationally deconvolute the individual profiles into constituent cell types by employing the same nBM used to define the heterogeneity in the CITE-seq data as a molecular reference, subsequently estimate their relative abundances, and relate to TKI response (Fig 3C). We used CIBERSORTx (Newman et al., 2019), a widely used algorithm, which has also been recently used to deconvolute bulk transcriptomes from acute myeloid leukemia (AML) (Zeng et al., 2022). As the gene expression profiles were measured at diagnosis from $CD34^{+}$ enriched cells from either bone marrow or

peripheral blood, this represented a cellular fraction broadly similar to ours for comparison. Importantly, the CML patient cohort was stratified by the percentage of Ph^+ cells after 12 months of Imatinib treatment as responders (0 % Ph^+ metaphases, complete cytogenetic response, CcyR) or non-responders (> 65 % Ph^+ metaphases, lack of even a minor cytogenetic response) as per the original study (McWeeney et al., 2010). We adhered to the patient annotation (responder or non-responder) provided by the original authors for consistency (see methods for more details).

The deconvolution results demonstrated a heterogeneous cell composition across patients, and overall comparison of imatinib non-responders (n = 18 out of 59) versus responders (n = 41 out of 59) showed a >3 fold statistically significant enrichment of primitive cells in non-responders (Fig. 3D, Supp. Fig. 3B). To assess whether the source of origin of $CD34^+$ cells in the public dataset could bias our results, we compared the abundances of imputed cell types from non-responders and responders based on their extraction from either bone marrow, or peripheral blood separately. This once again revealed a statistically enriched presence of primitive cells in non-responders versus the responders in the bone marrow (~3 fold higher). Moreover, and unlike the findings from overall comparison, myeloid cells were also found to be statistically enriched within responders (~2.5 fold higher) (Fig. 3E). Although MPP2 and MkP clusters showed increased abundance in non-responders and responders respectively, the difference did not reach statistical significance. Notably, the primitive cells were rarely detected in peripheral blood in contrast to the bone marrow, confirming the notion that cell type fractions differ in different tissues (Fig. 3D), and the bone marrow is predictably a more reliable and abundant source of true primitive cells in CML. Taken together, our analyses revealed distinct cellular heterogeneity across CML patients at diagnosis and highlighted that cell composition is associated with therapy response. Specifically, a higher burden of cells with a stem-like signature at diagnosis is a strong indicator of treatment failure.

Identification of BCR::ABL1$^+$ and BCR::ABL1$^-$ primitive cells and their surface markers by combining single-cell gene expression with ADTs

Interestingly, according to the ADT data the established CML stem cell markers CD25, CD26, and CD93 could only capture a fraction of the primitive cells (Supp. Fig. 3C). To further investigate the molecular and immunophenotypic heterogeneity within the primitive cluster we performed CITE-seq on the stem cell enriched $Lin^-CD34^+CD38^{-/low}$ compartment from the same patients (n = 8; 6,779 cells). A stepwise analysis (Fig. 4A) was performed to resolve the BCR::ABL1 status of the individual primitive cells and determine their immunophenotype. First (1), the primitive cells from the $Lin^-CD34^+CD38^{-/low}$ fraction of all CML patients were merged and classified by BCR::ABL1 status using publicly available BCR::ABL1$^+$ gene signatures. Next (2) CITE-seq data from both the Lin^-CD34^+ and the $Lin^-CD34^+CD38^{-/low}$ sorted population from the same patient was merged and visualized in a joint UMAP, while (3) the BCR::ABL1 status of the $Lin^-CD34^+CD38^{-/low}$ primitive cells was linked to the merged UMAPs by cell ID. Finally (4) the log2 fold change in ADT expression between

BCR::ABL1$^+$ and BCR::ABL1$^-$ primitive cells were calculated and the remaining cells of the UMAP were color-coded by the cluster identity generated by label-transferred projection to nBM.

The BCR::ABL1 status of the primitive cells was determined using two previously established gene expression signatures comparing Lin$^-$CD34$^+$CD38$^{-/low}$ BCR::ABL1$^+$ LSCs to normal Lin$^-$CD34$^+$CD38$^{-/low}$ HSCs, and Lin$^-$CD34$^+$CD38$^{-/low}$ BCR::ABL1$^-$ non-leukemic stem cells (Giustacchini et al., 2017). These signatures have been derived by analyzing cells with SMART-seq for global transcriptome, and primers specific to the BCR::ABL1 fusion gene, simultaneously and therefore represent useful anchors to query and label cells as either BCR::ABL1$^+$ or BCR::ABL1$^-$ (See methods for detailed analysis).

In the UMAP generated from all Lin$^-$CD34$^+$CD38$^{-/low}$ primitive cells, we identified three coarse clusters, where two consisted of primitive CML cells with representation from all patients (cluster 2-3), and one represented Lin$^-$CD34$^+$CD38$^{-/low}$ primitive cells from nBM which were included as negative control (cluster 1) (Supp. Fig. 4B-C). When we queried each cluster for enrichment of either LSC or HSC-like gene signatures the analysis clearly demonstrated that the primitive cells from CML samples could be divided based on the presence of BCR:ABL1, where CML cluster 3 displayed an evident enrichment of BCR::ABL1$^+$ LSC specific signatures as compared to CML cluster 2 consisting of BCR::ABL1$^-$ non-leukemic stem cells (Supp. Fig. 4 D-E). Interestingly, both CML clusters were also found to share gene characteristics with normal stem cells (Supp. Fig. 4 D). Accordingly, we annotated Lin$^-$CD34$^+$CD38$^{-/low}$ primitive cells from individual patients as either BCR::ABL1$^+$ or BCR::ABL1$^-$ and could observe that the distribution varied across patients, suggesting a variable load of leukemic stem and normal stem-like cells within the primitive fraction (Supp. Fig. 4F).

Remarkably, subsequent matching of BCR::ABL1$^+$ and BCR::ABL1$^-$ cell IDs to the primitive cells in the joint Lin$^-$CD34$^+$ and Lin$^-$CD34$^+$CD38$^{-/low}$ UMAPs (indicated by red and black cell color, respectively), indeed revealed that BCR::ABL1$^+$ LSCs and BCR::ABL1$^-$ HSCs were distinctly and consistently separated in the UMAP for each patient (Fig. 4B, Supp. Fig. 5). BCR::ABL1$^+$ LSCs in all patients were positioned immediately juxtaposing the downstream progenitor populations forming a continuum of differentiation hierarchy characteristically observed in single-cell analysis of HSPCs (Pellin et al., 2019; Safi et al., 2022; Velten et al., 2017). In contrast, BCR::ABL1$^-$ HSCs formed an isolated and distinct cluster clearly detached from the rest of the cells in the majority of patients, indicating that during the chronic phase of CML, active hematopoiesis is dominated by the BCR::ABL1$^+$ LSCs while BCR::ABL1$^-$ HSCs reside in the bone marrow albeit in an inactive state with reduced contribution to hematopoiesis as previously suggested (Chen et al., 2023; Coulombel et al., 1983). Moreover, using the ADT data we could validate the molecularly defined BCR::ABL1$^+$ LSCs also by surface expression, with CD26, CD25, and CD93 displaying a 2-8 fold elevated expression in BCR::ABL1$^+$ primitive cells as compared to BCR::ABL1$^-$. A

noteworthy patient-specific variability in surface protein expression on the most primitive cells was also established (Fig. 4B).

To gain understanding of the nature of molecular program of BCR::ABL1$^+$ vs. BCR::ABL1$^-$ primitive cells, we analyzed differentially expressed genes between the pooled primitive BCR::ABL1$^+$ and BCR::ABL1$^-$ populations from all CML patients. This identified 244 genes specifically upregulated in BCR::ABL1$^+$ and 180 genes upregulated in BCR::ABL1$^-$ cells (Fig. 4C, Supp. Table 7). Interestingly, among genes up-regulated in BCR::ABL1$^+$ primitive cells included the expression of established CML markers; IL2RA (CD25), DPP4 (CD26) and IL1RAP as well as LEPR (CD295) a receptor recently described as a novel marker for Lin$^-$CD34$^+$CD38$^{-/low}$ LSCs (Landberg et al., 2018). In contrast, BCR::ABL1$^-$ cells displayed an up-regulated expression of the stem cell related gene CRHBP (Barbieri et al., 2022; He et al., 2005) as well as CXCR4 important for homing and maintenance of normal HSCs (Sugiyama et al., 2006). Upon applying the gene signatures to Lin$^-$CD34$^+$ cells, we could clearly identify as well as partition primitive cells into BCR::ABL1$^+$ vs. BCR::ABL1$^-$ (Fig. 4D and Supp. Fig. 6). This is especially relevant as the Lin$^-$CD34$^+$ fraction contains a higher proportion of lineage progenitors but a smaller fraction of primitive cells making their identification challenging. Taken together, this multistep analysis approach generated unique detailed UMAPs allowing for inspection of BCR::ABL1$^+$ LSCs and BCR::ABL1$^-$ HSCs, their relation to other progenitor cells, as well as further validate BCR::ABL1$^+$ LSCs identity by surface protein expression.

A unique combination of CD26 and CD35 surface markers captures molecularly defined BCR::ABL1$^+$ LSCs and BCR::ABL1$^-$ HSCs

A long-sought aim in CML research has been to generate protocols for effective discrimination and isolation of CML LSCs from residual HSCs within individual patient bone marrow. The single cell multiomic feature space of CITE-seq together with the identification of molecular distinct BCR::ABL1$^+$ LSCs and BCR::ABL1$^-$ HSCs provides a unique opportunity to identify efficient protocols for their separation.

To specifically define the surface markers for their ability to capture BCR::ABL1$^+$ vs. BCR::ABL1$^-$ primitive cells, we compared significantly up-regulated ADTs for either Lin$^-$CD34$^+$CD38$^{-/low}$ BCR::ABL1$^+$ LSCs or BCR::ABL1$^-$ HSCs cells across patients and identified markers with consistent expression across the data set. We found 28 unique markers to be significantly up-regulated for either BCR::ABL1$^+$ or BCR::ABL1$^-$ cells (black or red colored bars in Fig. 4B, Fig. 5A). Of these 28 markers, 17 ADTs marked BCR::ABL1$^+$ LSCs and were detected in at least one patient. However, only CD26, and CD25 were explicit and consistent throughout the entire cohort. CD93 was present on BCR::ABL1$^+$ LSCs in 7/8 patients and other previously suggested LSC markers like CD33 and CD56 specifically labeled BCR::ABL1$^+$ primitive cells in only a fraction of the patients. The documented CML LSC marker IL1RAP was not in the ADT panel and hence could not be probed. In contrast, 11 ADTs were specifically

detected in BCR::ABL1$^-$ primitive cells from at least one patient. Interestingly, CD35 with ~4-fold elevated expression as compared to BCR::ABL1$^+$ LSCs was the only marker found to be consistently specific for the BCR::ABL1$^-$ HSC population across all patients. CD62L and CD10 were specifically present on BCR::ABL1$^-$ HSCs in 6/8 and 5/8 patients, respectively. Intriguingly, we recently showed that CD35 captures all HSCs in healthy human hematopoiesis and that stem cell activity as measured by xenotransplantation assays and epigenetic profiling is restricted to CD35$^+$ HSCs (Sommarin et al., 2021). By applying the BCR::ABL1 signatures also to the Lin$^-$CD34$^+$ primitive cells (Supp. Fig. 7), we could visualize the relative expression within the Lin$^-$CD34$^+$ UMAPs in relation to the cells BCR::ABL1 status and further confirm that the primitive fraction, previously captured by the established CML stem cell markers CD25, CD26, and CD93, consisted of specifically BCR::ABL1$^+$ LSCs (Fig. 5 B-C, Supp. Fig. 8 and 9A). In addition, we observed that our previously described surface marker CD117, whose absence characterized LSCs persisting 3 months of TKI therapy, displayed a highly variably expression at diagnosis both marking a proportion of LSCs and HSCs across patients. Interestingly, despite that relative expression of CD35$^+$ was lower in the primitive cells compared to MEP/ERP cell clusters the CD35$^+$ gate captured ~50% of the BCR::ABL1$^-$ primitive cluster.

Given the consistency of detection across patients, we specifically focused on the ability of ADTs against CD25, CD26 and CD35 to separate between BCR::ABL1$^+$ LSCs and BCR::ABL1$^-$ HSCs within the stem cell-enriched Lin$^-$CD34$^+$CD38$^{-/low}$ compartment. CD26 showed the highest capture of the BCR::ABL1$^+$ primitive cluster (>95%) with a consistent capture percentage across patients (Fig. 5D). This was followed by CD25 which captured >80% of the BCR::ABL1$^+$ primitive cluster on average but displayed higher variability in capture efficiency compared to CD26 across patients. In comparison, the percentage of BCR::ABL1$^-$ primitive cluster captured by CD26 and CD25 was considerably lower (~5%). In contrast, the CD35+ gate showed a remarkable specific capture of BCR::ABL1$^-$ primitive cluster (~50%) (Fig. 5D).

To further confirm whether CD26 and CD35 together could efficiently separate BCR::ABL1$^+$ and BCR::ABL1$^-$ primitive cells, we gated for different combinations of CD26 and CD35 within the Lin$^-$CD34$^+$CD38$^{-/low}$ compartment (Fig. 5E, Supp. Fig. 9B). Predictably, whereas a combination of CD26$^+$CD35$^-$ ADTs captured BCR::ABL1$^+$ primitive LSC cluster at high purity, the CD26$^-$CD35$^+$ combination marked BCR::ABL1$^-$ primitive HSC cluster with no contamination of BCR::ABL1$^+$ LSCs (Fig. 5E). Interestingly, CD35 expression divided the CD26$^-$, BCR::ABL1$^-$ primitive cells in one CD35+ and one CD35- fraction. This is in line with our recent observation that human BM immunophenotypic stem cells can be divided by CD35, where all HSC activity is captured within the CD35$^+$ fraction (Sommarin et al., 2021). Accordingly, ADT combination of CD26$^-$CD35$^-$ captured BCR::ABL1$^-$ primitive cells likely representing non-leukemic MPPs downstream of normal CD26$^-$CD35$^+$ stem cells. Notably, only a minority of cells were positive for ADTs for the CD26$^+$CD35$^+$ combination as evidenced by an overall low capture of cells in general. Thus, this shows

the importance for positive, HSC-specific markers for efficient isolation of CML LSCs, and detection of residual HSCs in leukemia. Taken together, these observations suggested that although patients are heterogeneous for a given marker, BCR::ABL1$^+$ LSCs can be consistently captured by the CD26$^+$CD35$^-$ combination while BCR::ABL1$^-$ HSCs expressed a CD26$^-$CD35$^+$ immunophenotype within Lin$^-$ CD34$^+$CD38$^{-/low}$ compartment in the bone marrow of CML patients.

A comparative analysis of CD26$^+$CD35$^-$ versus CD26$^-$CD35$^+$ cells for BCR::ABL1 expression and response to TKI therapy

To explore whether the combination of CD26 and CD35 could indeed purify BCR::ABL1$^+$ vs. BCR::ABL1$^-$ in Flow Cytometry protocols, we sorted CD26$^+$CD35$^-$ and CD26$^-$CD35$^+$ cells from the Lin$^-$CD34$^+$CD38$^{-/low}$compartment from patients both before and following 3 months of Bosutinib therapy and employed quantitative real time qPCR analysis using Taqman probes against the BCR::ABL1 fusion gene (Fig. 6A). The analysis showed a strong signal within CD26$^+$CD35$^-$ cells for BCR::ABL1 expression while CD26$^-$CD35$^+$ cells were BCR::ABL1$^{low/negative}$, validating the capacity of the combination of CD26 and CD35 to separate BCR::ABL1$^+$ and BCR::ABL1$^-$ stem cells at diagnosis as well as after 2nd generation TKI therapy. In addition, real time qPCR analysis confirmed that Lin$^-$CD34$^+$CD38$^{-/low}$CD26$^+$CD35$^-$ cells from CML patients at diagnosis displayed a strong signal for GAS2 (Fig. 6B), one of the top genes from the CITE-seq BCR::ABL1$^+$ LSC signature (Fig. 4C). Furthermore, CD26$^+$CD35$^-$ cells maintained GAS2 expression following 3 months of Bosutinib therapy (Fig. 6B). GAS2 has previously been linked to CML disease progression, cell cycle control, apoptosis, and response to Imatinib (Janssen et al., 2005; Radich et al., 2006; Zhou et al., 2014).

To assess the level of quiescence between the BCR::ABL1$^+$ LSCs and BCR::ABL1$^-$ HSCs (Nakamura-Ishizu et al., 2014), we sorted Lin$^-$CD34$^+$CD38$^{-/low}$CD45RA$^-$ CD26$^+$CD35$^-$ and CD26$^-$CD35$^+$ single cells from two CML patients at diagnosis into individual wells and examined their division kinetics for 140 hours. However, LSC and HSC populations were indistinguishably deeply quiescent with average times to first division of 80-100 hour in culture (Supp. Fig. 9C-D). Moreover, cell cycle analysis was performed by gating the corresponding cell populations in the Lin$^-$CD34$^+$CD38$^{-/low}$ CITE-seq data using ADTs. In accordance with the *in vitro* study, there was no distinct difference in cell cycle status between the populations (Supp. Fig. 9E-F).

The higher burden of primitive cells in treatment failures observed above prompted us to query to which extent patients differed in the load of isolatable BCR::ABL1$^+$ vs. BCR::ABL1$^-$ at diagnosis and their sustenance in response to TKI therapy. Intriguingly, we noted a substantially higher ratio of CD26$^+$CD35$^-$ LSCs over CD26$^-$CD35$^+$ HSCs at diagnosis in prospective treatment failures compared to the bone marrow of optimal responders, both using CITE-seq ADTs as well as in FACS analysis for CD26 and CD35 (Fig. 6C-D, Supp. Fig. 9B). Importantly, following 3 months of TKI therapy, the percentage of BCR::ABL1$^+$ CD26$^+$CD35$^-$ cells decreased in both groups of patients;

however, there was a striking difference in the relative proportion of $CD26^{+}CD35^{-}$ LSCs/$CD26^{-}CD35^{+}$ HSCs in both groups. The stem cell compartment of optimal responders was dominated by healthy HSCs at three months following treatment. In contrast, the stem cell population of failure patients still comprised of $CD26^{+}CD35^{-}$ LSCs without re-establishment of HSCs and restoration of normal hematopoiesis (Fig. 6E). Taken together, we here for the first time present a protocol for separation and isolation of both BCR::$ABL1^{+}$ LSCs and BCR::$ABL1^{-}$ HSCs from the same CML patients, two populations evidently relevant to therapy response.

Discussion

As new and more potent TKIs continue to be developed (Braun et al., 2020), the persistence of fully leukemogenic cells even in TFR necessitates life-long therapy in most patients. The ensuing treatment-emergent adverse events, and financial toxicity (Cortes et al., 2021; Lipton et al., 2022; Zafar, 2016) motivate a search for organizing principles to predict therapy response, dampen disease progression and achieve durable TFR in a larger fraction of CML patients. One recent development has been to invoke the presence of somatic mutations other than BCR::ABL1 to explain primary resistance to TKIs, and disease progression (Branford et al., 2019). A complementary perspective is to consider leukemic cell state and heterogeneity as a fundamental determinant of response to TKI to augment the mutational foundation, as has been recently demonstrated in AML (Zeng et al., 2022).

Our single cell multiomics maps show clear differences in overall cell composition within stem and progenitor compartments in leukemia patients at diagnosis versus nBM. Importantly, treatment failures and optimal responders displayed distinctive enrichment of specific cell clusters. Using our 11-molecularly defined clusters as anchors, we deconvoluted the bulk gene expression profiles from n=59 CML patients to infer constituent cell populations and found that a more profound stemness/primitive signature in the BM consistently associated with inferior therapy response. Indeed, there is growing recognition of the burden of primitive cells, and the ratio of BCR::$ABL1^{+}$ vs. BCR::$ABL1^{-}$ within the primitive compartment as potentially clinically relevant features such as hemoglobin, blast count, overall survival, progression free survival, and therapy response (Fathy El-Metwaly et al., 2021; Krishnan et al., 2023; Mustjoki et al., 2013; Thielen et al., 2016). Apart from the differential burden, the primitive cells from optimal and sub-optimal responders could also be qualitatively different e.g., in terms of gene expression profile as suggested recently (Krishnan et al., 2023). The relevance of BCR::$ABL1^{+}$ LSC burden to 1^{st} and 2^{nd} generation TKI therapy outcome stands in contrast to the leukemic progenitors (Ph^{+} $CD34^{+}CD38^{+}$) which did not show such correlation (Mustjoki et al., 2013). Moreover, longstanding observations have revealed that CML patients at diagnosis contain both BCR::$ABL1^{+}$ LSCs vs. BCR::$ABL1^{-}$ HSC within the $Lin^{-}CD34^{+}CD38^{-/low}$ immunophenotypic compartment, and BCR::$ABL1^{+}$ LSCs suppress residual normal HSCs (Chen et al., 2023; Coulombel et al., 1983). Predictably, a lower fraction of BCR::$ABL1^{-}$ normal stem cells at diagnosis and during therapy relates to hematological

toxicity with delayed or compromised restoration of Ph^{neg} hematopoiesis upon successful response to TKIs (Janssen et al., 2012). Here, we for the first time present an effective means to separate CML LSCs from HSCs within the stem cell compartment of patients. Prospective optimal responders to TKI treatment had a higher content of $BCR::ABL1^{-}CD26^{-}CD35^{+}$ cells at diagnosis, and 3 months following therapy versus the treatment failures. We have recently demonstrated that $Lin^{-}CD34^{+}CD38^{-/low}CD45RA^{-}CD35^{+}$ cells are at the top of human hematopoietic hierarchy and display chromatin accessibility and transcriptional enhancers in line with their multilineage long-term reconstitution ability (Sommarin et al., 2021).

With the high-throughput and resolution now provided by single cell methods, $BCR::ABL1^{+}$ cells can be distinguished from $BCR::ABL1^{-}$ cells residing within the same immunophenotypic compartment as described above, and importantly, heterogeneity within $BCR::ABL1^{+}$ LSC subpopulations in terms of cell surface markers, molecular signature, and TKI response can be measured. The use of CITE-seq enabled generation of patient-specific maps providing a panoramic yet exquisitely detailed view of cellular heterogeneity. Intriguingly, one of the emerging principles from the single cell studies has been that not all LSC subpopulations are equally sensitive to BCR::ABL1 inhibition; while a majority of the LSCs are depleted, at least a fraction survives (Giustacchini et al., 2017; Warfvinge et al., 2017). This is corroborated by overall reduction in $BCR::ABL1^{+}$ $Lin^{-}CD34^{+}CD38^{-/low}$ cells but a striking enrichment of $cKIT^{-}CD26^{+}$ subpopulation displaying primitive and quiescent molecular program upon commencing TKI therapy (Warfvinge et al., 2017). Using CITE-seq, we confirmed the existence of these cells already at diagnosis and showed that $BCR::ABL1^{+}$ vs. $BCR::ABL1^{-}$ can be efficiently discriminated as $CD26^{+}CD35^{-}$ and $CD26^{-}CD35^{+}$ respectively within the $Lin^{-}CD34^{+}CD38^{-/low}$ fraction, and thus facilitating improved assessment of LSC burden.

The inspection of single cell maps raises questions both regarding the origin of the interpatient heterogeneity in LSC burden as well as how these cells differentially manage to survive TKI therapy. Given the heterogeneity within normal HSCs with respect to lineage bias and clonal output (Haas et al., 2018), it is tempting to speculate that stem/progenitor cell acquiring the BCR::ABL1 oncogenic hit perhaps might be different across CML patients ensuring disparity in LSC load and characteristics. An equally plausible alternative is variability in the bone marrow niche that might favor differential abundance of stem/lineage-biased progenitors in patients (Baryawno et al., 2017). Once established, at least a subset of the LSCs is likely to be independent of BCR::ABL1 kinase signaling for their survival (Bhatia et al., 2003; Corbin et al., 2011; Hamilton et al., 2012). However, whether their self-sustenance involves switching to non-kinase activity of BCR::ABL1 protein, or achieving total BCR::ABL1 independence, and whether such mechanisms are inherently active in treatment naïve cells or become active only after exposure to TKIs is poorly understood (Zhao & Deininger, 2020).

We foresee future investigations to provide several key insights. First, accurate and direct detection of fusion transcripts such as BCR::ABL1 in single cells as part of scRNA-seq remains a major constraint, however, new approaches should allow direct measurement of BCR::ABL1 on a massive scale. Second, CITE-seq, a single cell multiome approach, like any other high-throughput single cell method comes with methodological, technical, and biological challenges. Cell sample handling, library preparation, sequencing quality and depth, drop-out of lowly expressed genes, and taking a molecular 'snapshot' of cells in time are all merely some factors that could introduce variability and noise to the data. A simpler, faster, and cheaper FACS panel detecting $CD26^{+}$ and $CD35^{+}$ surface markers can possibly work as an applicable clinical tool to quantify leukemic and non-leukemic stem cells in CML patients. Future prospective studies of this FACS panel coupled to clinical trials in large patient cohorts will establish the diagnostic and prognostic value of the relative abundance of these populations. It will be of importance to evaluate if $CD26^{-}CD35^{+}$ cells are critical for restoring normal hematopoiesis once the TKI therapy diminishes the leukemic load, and whether patients with low counts of $CD26^{-}CD35^{+}$ cells at diagnosis have a relatively higher risk of developing hematologic toxicity such as cytopenia during therapy. The relative levels of $CD26^{-}$ and $CD35^{+}$ stem cells for TFR will also be an important area of investigation.

Third, joint longitudinal analysis of leukemic as well as immune compartments is likely to be informative especially for TFR. The observations that patients with activated immune signature at diagnosis are more likely to optimally respond to TKIs (Radich et al., 2023) serve as apt reminder for collective analyses. Fourth, our capacity to generate single cell datasets, ironically outpaces our ability to extract information. Development of tools that allow biologists and clinicians to analyze large scale datasets without requiring dedicated bioinformatics infrastructure can overcome the challenge (Dhapola et al., 2022). Finally, the clonal relationships and lineage output of candidate $BCR::ABL1^{+}$ LSC subpopulations remain unknown. By coupling sc-multiomics with barcoding analysis and lineage tracing (Wagner & Klein, 2020), it should be possible to evaluate, for instance, whether the $BCR::ABL1^{+}CD26^{+}$ cells detected in patients in TFR are a sub-clone that persists from diagnosis through therapy, and whether it is responsible for recurrence in TFR.

The notion of LSCs has been invoked for a long time in the genetically defined and molecularly targeted paradigm of CML (Holyoake & Vetrie, 2017). Still these entities remain essentially peripheral to the disease management (Zhao & Deininger, 2021). We posit that the heterogeneity of LSCs is a barrier towards their efficient measurement and safe purging. Our high-resolution single cell multiomics maps suggest how to probe and deconstruct heterogeneity of CML, thereby permitting inference of leukemic vs. non-leukemic cells, estimation of $BCR::ABL1^{+}$ LSCs, enumeration of their molecular features, and prospective isolation. Understanding how the cellular heterogeneity and plasticity emerges in the absence of extensive genetic variability would inform if the fully leukemogenic residual cells could either be safely eliminated pharmacologically

or kept perpetually suppressed by empowered immune system to avoid recurrence (Hsieh et al., 2021; Zhao & Deininger, 2023). Alternatively, longitudinal sampling and sc-omics combined with barcoding may also reveal if the stem cell subpopulations and states are interconvertible (Lenaerts et al., 2010; Marjanovic et al., 2013), and therefore appear as potentially inexhaustible pool that can only be slowly eroded by several years of TKI treatment in a subset of patients. A more formidable barrier is the unstated but still presumed equivalence of immunophenotype and function. Rather than describing LSCs solely by surface markers, we propose that treating leukemic cellular clones as the fundamental units of selection and evolution during therapy would have a more meaningful impact in predicting response to existing therapy and switch to another TKI. The next line of advances will require assessing LSCs as pool of clones defined by their ability to contribute to primary and secondary resistance in patients on therapy, and recurrence in TFR without recourse to animal models.

Materials and methods

Patient samples

The bone marrow was obtained from patients enrolled in either BosuPeg clinical trial (NCT03831776), NordCML006 (NCT00852566), BFORE (NCT02130557), or from Skåne University Hospital, Lund after informed consent and processed according to the guidelines approved by regional research ethics committees of sites involved in the trial. The information on age, gender, TKIs, BCR::ABL1^{IS} % and therapy response as per ELN guidelines are provided as supplementary table 1. MNCs or CD34^{+} cells were enriched from the BM aspirates using magnetic microbeads and subsequently cryopreserved. The collection, processing and generation of CITE-seq of bone marrow from age matched healthy donors used in this study has been described previously (Sommarin et al., 2021).

CITE-seq sample preparation and FACS Sort

Sample preparation was performed according to (Stoeckius et al., 2017) with minor adaptations. In brief, CML MNC or CD34 enriched BM samples was thawed, FCR blocked 1/5 (130-046-703, Miltenyi) for 10 min and washed before staining. Samples were stained with a PeCy5 conjugated lineage cocktail (CD2, CD3, CD14, CD16, CD19, CD235a), CD34 FITC, and a subset of the CITE-seq panel for 30 min on ice. Samples were washed and split into two tubes and stained with either CD38-PeCy7 or CD38-CITE-seq antibody followed by individual hashtags and the rest of the CITE-seq panel for 30 min on ice (Supp. Table 2 and 3). Cells were washed and resuspended in PBS, 2 % FBS, 1/100 7AAD (Hyclone, 559925, BD Bioscience). Two populations (Lin^{-}CD34^{+} and Lin^{-}CD34^{+}CD38$^{-/low}$) were sorted per sample using FACSAriaII/Aria III (BD Bioscience) into 300 µl PBS, 0.04 % BSA. Sorted cells were centrifuged at 300 x g for 10 min and volume was adjusted to 45 µl.

CITE-seq library preparation and sequencing

CITE-seq library preparation and sequencing Cells were processed through Chromium Controller (10x Genomics) with a total of 20-30.000 cells loaded per lane. Single-cell cDNA, HTO (Hashtags) and ADT (CITE-seq antibodies) libraries was prepared using Chromium Single Cell 3' V3 as per manufacturer instructions (CG000183 Rev C) as reported previously (Stoeckius et al., 2017). In brief, to increase HTO and ADT library yield, HTO and ADT specific primers were spiked-in during the cDNA amplification step. cDNA and HTO/ADT libraries were isolated using 2X SPRI beads per manufacturers protocol. HTO and ADT libraries were subjected to adaptor ligation and sample index in separate PCRs using KAPA Hifi PCR Readymix (10 and 11 PCR cycles respectively). The cDNA library was subjected to fragmentation, end repair, A-tailing, adaptor ligation and sample index PCR (12 cycles). cDNA, HTO and ADT libraries were sequenced together (65 % cDNA, 30 %ADT, 5 % HTO) on Illumina sequencers with the following read length configuration: Read1=28, i7=8, i5=0, Read2=91. The raw data was processed using Cell Ranger 3.0.2 with GRCh38 as a reference genome.

CITE-seq analysis

Cell-gene matrices produced by Cell Ranger were analyzed using Scarf (v.0.18.12) (Dhapola et al., 2022). In brief, cells with low or high gene count (<1000 or >9000 genes) and cells with high percentage mitochondrial gene UMIs (>11 % or >6 % for CML samples and healthy BM reference, respectively) were excluded from the analysis. The matrices were demultiplexed using Otsu thresholding (automatized pixel-based thresholding of HTO count per cell, background buffer = 0.1, override value = 0.5) (Otsu thresholding was run twice for CML4, CML9. For nBM the thresholds were adjusted to HTO_1 = 32, HTO_2 = 18, HTO_3 = 17). HTO UMAPs were generated through Scarf (dims = 0) and clustered with Paris clustering (n_clusters = 2). If any RNA leiden cluster overlapped with HTO paris cluster > 70 % and conversely, it was considered doublets and excluded from analysis.

Post-demultiplexing, for each sample, 2000 highly variable genes (HVGs) were identified (min_cells = 50) with the "mark_hvgs" function in Scarf and used for PCA (principal component analysis) (CML8; HVGs = 1000, min_cells = 30). KNN (K-Nearest Neighbors) graphs were calculated based on the top 20 principal components (n_neighbours = 11) and utilized to build UMAP embedding of the cells (min_dist=1, spread=2, n_epochs= 2000). Clustering was performed using Lieden clustering (resolution set to 1 and 0.76 for CML and nBM samples respectively).

Projection of $Lin^{-}CD34^{+}$ and $Lin^{-}CD34^{+}CD38^{-/low}$ CML subpopulations

Mapping reference

The nBM is merged CITE-seq data of two $Lin^{-}CD34^{+}$ FACS sorted bone marrow samples (Sommarin et al., 2021) reanalyzed as described above'. Cluster identity was

determined by (a) the top 10 genes in "run_ marker_search" function in Scarf. In brief, each genes expression value is ranked per cell and a gene's mean rank per cluster is divided by the sum of mean to determine the cluster specificity, (b) CLR (centred-log ratio) normed ADT expression across cluster was used to determine the immunophenotypic identity the cells, and (c) cell cycle scoring using the "run_cell_cycle_scoring" function in Scarf was used to estimate cell cycle phase.

Label transfer through reference-based cell projection

CML subpopulations were mapped to Lin$^-$CD34$^+$ nBM using Scarf (v.0.18.12). In short, cells were projected using 'K-Nearest Neighbours (KNN) mapping through Scarf's "run_mapping" function (neighbours = 5). Cell cluster identity for CML cells was determined using the "get_target_classes" function with threshold set to 0.5 (> 50 % of the total weight score from the five top matched reference cells must be cluster specific to assign identity). Mapping scores (how frequently the reference cells end up as one of top 5 neighbours of the projected CML cells) for the individual reference cells was calculated per projected sample using "get_mapping score". To visualize the mapping score and compare the mapping across samples, cells size of reference cells was set proportional to the score in the healthy bone marrow reference UMAP.

Following mapping of Lin$^-$CD34$^+$CD38$^{-/low}$ CML cells (n = 8), the primitive clusters from all patients were merged in Scarf. The "make_graph" function in Scarf was used to identify the primitive CMLs cells top 500 HVGs (min_cells =30, gender specific genes excluded). Lin$^-$CD34$^+$CD38$^{-/low}$ healthy bone marrow cells (n = 1) were projected onto the healthy reference as described above and the primitive cluster was added to the primitive CML cell clusters in Scarf. The UMAP was generated using the 500 CML specific HVGs (k =11, PC = 20, n_epoch = 500) and with PCA fitted to the primitive CML cells only using Scarf's "make graph" function. Subsequently, cells were clustered using Leiden clustering method (resolution = 0.1).

BCR::ABL1 status of the primitive clusters was determined using two DEG signatures: (1) Normal HSC vs BCR::ABL1$^+$, and (2) BCR::ABL1$^-$ vs BCR::ABL1$^+$ where Lin$^-$CD34$^+$CD38$^{-/low}$BCR::ABL1$^+$ cells have been validated through single-cell RT-qPCR (Giustacchini et al., 2017). Up- and down-regulated genes were defined as log2 fold change > 1 and < 0, respectively. The expression of signature genes was normalized in Scarf, Z-scored to provide an average value count of the signature per cell and visualized in the UMAP using Scarf.

To visualize the BCR::ABL1$^+$ primitive cells alongside the full CML heterogeneity, Lin$^-$CD34$^+$ and Lin$^-$CD34$^+$CD38$^{-/low}$ CML CITE-seq data from the same patient sample was merged in Scarf (The sub populations were FACS sorted at the time point and sequenced together). UMAPs of the merged data sets were generated as previously described (2000 HVGs, neighbours = 11, PC = 20). Cell indexes from BCR::ABL1$^+$ and BCR::ABL1$^-$ primitive CML clusters was matched to the Lin$^-$CD34$^+$CD38$^{-/low}$ cell data.

ADT expression of BCR::ABL1^{+} and BCR::ABL1^{-} cells were retrieved from the zarr file in Scarf. The data thereafter was CLR (centered-log ratio) normalized and the log2 fold change was calculated between the two groups of cells using mean expression. P-values were calculated with Mann–Whitney U test and they were corrected for multiple hypotheses testing using Bonferroni method.

Analysis of differentially expressed genes

DESeq2 was used to identify differentially expressed genes. Significantly up- or down-regulated was selected based on adjusted p-value < .01 and log2 fold change > 1 or < -1. Subsequently, volcano plots showing log2 fold change and -Log10 p-values were generated. Mitochondrial/ribosomal genes, as well as genes with a total count below 10 was excluded from the analysis.

To compare gene expression between clusters 1 to 11 from Lin^{-}CD34^{+} CML cells, n = 9) and their normal counterparts, their corresponding normal bone marrow reference clusters (n =2) were randomly pseudo bulked into 3 replicates. Cluster specific signatures genes were defined as significant up- or down-regulated genes unique to the cluster comparison, and not shared with not any other clusters. CML signature genes were defined as significantly up- or down- regulated genes present in all 11 clusters. Heatmap was generated from the DEseq2 data output (VST), showing the log2 mean expression of all samples per cluster. BCR::ABL1^{+} and BCR::ABL1^{-} clusters > 25 cells was used for DEG analysis of Lin^{-}CD34^{+}CD38$^{-/low}$ primitive cells (n = 7).

ADT gating

ADT expression was CLR *(centered-log ratio)* normalized in Scarf. The normalized data was transformed into its antilog, multiplied with a scaling factor of 1000 and exported as FCS files. The FCS files was analysed using FlowJo software. Gated cells ADT scale values were exported as CSV files and matched to cells ADT expression in CITE-seq data to determine original cell identity.

Gene expression deconvolution

The gene expression counts from CITE-seq molecularly defined populations served as input for CIBERSORTx (Newman et al., 2019) at default settings run on its docker version. Deconvolution of publicly available CD34^{+} bulk gene expression microarray dataset GSE14671 (McWeeney et al., 2010) was performed after robust multichip average (RMA) normalization (Irizarry et al., 2003). Upon estimation of relative abundances of subpopulations from CD34^{+} cells, the values were normalized to 1, the value for each subpopulation represented its percentage/fraction within the query sample. Individual patients were annotated as non-responders or responders to Imatinib therapy as defined in the original study (McWeeney et al., 2010); non-responders with >65% Ph+ metaphases (the patients did not achieve even a minor cytogenetic response as described by the original authors), responders with 0% with Ph+ metaphases (achieved CCyR) after 12 months of Imatinib therapy. Notably, the threshold for

defining therapy response was proposed by the original authors and the patients were labeled as either responder or non-responder (McWeeney et al., 2010). We adhered to the patient labels provided by the original authors as described in GSE14671.

Flow cytometry for phenotyping

Lymphoprep kits were used to separate mononuclear cells (MNCs), and magnetic microbeads were used to enrich $CD34^+$ cells (Miltenyi). Antibodies against lineage-specific markers and those for specific populations mentioned in Supplementary Table 3 were used to stain the cells. Sorting and analysis were done using FACS ARIAII/III or LSR FORTESSA (BD Biosciences); data analysis was done with FlowJo (Tree Star)

qPCR for BCR::ABL1

RNA from FACS sorted cells was purified using Single Cell RNA Purification Kit (Norgen, cat# 51800) followed by cDNA synthesis using High-Capacity cDNA Reverse Transcription Kit (Applied Biosystems, cat# 4368814). Following pre-amplification of cDNA (SsoAdvanced PreAmp Supermix (BioRad, cat# 172-5160) for 12 cycles, qPCR was performed with TaqMan gene expression master mix (Applied Biosystems, cat# 4369016) and TaqMan probes for BCR::ABL1 (Assay ID: Hs03024541_ft), GAS2 (Assay ID: Hs00169477_m1 and GAPDH (Assay ID: Hs02758991_ft).

Time to first division in vitro

$Lin^-CD34^+CD38^{-/low}CD45RA^-CD26^+CD35^-$ or $CD26^-CD35^+$ BM single cells from two CML patients were sorted into individual wells of 96-well U shaped-bottom TPP plates using the FACS Aria III flow cytometer (Becton Dickinson). Cells were sorted directly into 200 µl Stem Span Serum-Free Expansion Medium (SFEM, StemCell Technologies), supplemented with 100 units/ml penicillin, 0.1 mg/ml streptomycin (Hyclone) and the following cytokines from PeproTech: SCF (100 ng/ml), Flt3L (100 ng/ml), TPO (50 ng/ml), and IL7 (10 ng/ml). Cells were visualized and counted in each well thrice a day using an inverted microscope for >140 hours. Dead cells as well as cells that did not divide during this period were excluded from the analysis. The Curve fit-sigmoid approach in GraphPad Prism was used to analyze the data.

Data availability

The data from sequencing have been submitted to GEO under accession ID: GSE236233 and are publicly available as of the date of publication. Previously published data used within this study is available at: GSE173076 (nBM), GSE1467 (deconvolution).

Author contributions

RW, GK, and RKT conceived and designed the study, that was supervised by GK; RW designed the CITE-seq ADT panel with inputs from MNES, LGU, RKT, and GK. CITE-seq experiments were performed by RW with help from LGU; FACS, and qPCR

analysis were done by LGU, in vitro cell division kinetics measurements were recorded by LGU and FS with contribution from GK, RKT and RW. CITE-seq analysis was done by RW with assistance from PD, bulk gene expression deconvolution analysis was implemented by SS with assistance from GK and RKT. JR, HHjH, and SM provided patient material and data from the clinical trials as well as interpretation of data and advice. RW summarized the data and generated the figures. RW, RKT and GK wrote the manuscript with input from all authors. All authors read and approved the final version.

Conflict of interest disclosure

GK and PD are board members and have equity in Nygen Analytics AB, JR reports receiving honoraria and research funding from Novartis and Bristol-Myers Squibb (BMS) and honoraria from Ariad. HHjH has received honoraria from Pfizer, Novartis, BMS, and Incyte. SM has received honoraria and research funding from BMS, and research funding from Novartis, Janpix, and honoraria from Dren Bio. Sample collection from patients in the BosuPeg and BFORE clinical trials was supported by Pfizer investigator grant. Other honoraria, and research funds were for projects unrelated to this study. The remaining authors declare no conflicts of interest.

Acknowledgements

We would like to acknowledge patients, study nurses, and other personnel in the clinical centers for their participation in this project. We also thank Clinical Genomics Lund, SciLifeLab and Center for Translational Genomics (CTG), Lund University, for providing expertise and service with sequencing and analysis, and the Lund Stem Cell Center FACS Facility for expert Flow Cytometry technical support. This work was funded by grants from the Swedish Cancer Society, the Ragnar Söderberg Foundation, the Knut and Alice Wallenberg Foundation, the Swedish Research Council, the Swedish Childhood Cancer fund, and a grant from Incyte Biosciences Nordic AB.

Figure legends

Main figures

Figure 1. Single cell multiomics analysis of CML and normal bone marrow (nBM) by CITE-seq

A. CML LSC and progenitor populations from nine CML BM samples at diagnosis were FACS sorted and subjected to CITE-seq. CML heterogeneity was defined by label transfer through cell projection onto a reference UMAP of age-matched nBM from two donors (Sommarin et al., 2021). Diagnostic samples were retrospectively stratified by BCR::ABL1 International Scale (IS) % after 12 months of TKI treatment, according to the European LeukemiaNet recommendations.

(B) UMAP embedding of 4,696 Lin$^-$CD34$^+$ nBM cells (n = 2) with 11 clusters identified by Leiden clustering; annotated by marker genes and ADT expression (HSC = hematopoietic stem cell; MPP = multipotent progenitor population 1; My/Ly = myeloid, lymphoid progenitors; My = myeloid progenitors; Ly/pDC/mono = lymphoid, dendritic, monocytic progenitors; MPP2 = multipotent progenitor population 2; MEP = megakaryocytic erythroid progenitors); MkP = megakaryocytic erythroid progenitors; ErP = erythroid progenitors; Baso/mc = basophilic, mast cell progenitors; Cycling = Cycling progenitors). The bar plot below shows the percentage of cells per cluster.

(C) Dot plot showing the ADT expression within clusters. The color indicates mean ADT expression (red = high expression, blue = low expression); dot size represents the fraction of cells with expression.

(D) Dot plot showing mRNA expression of the top 10 marker genes per cluster. The color indicates mean RNA expression (red = high expression, blue = low expression); dot size represents the fraction of cells with expression.

Figure 2. Single cell maps of heterogeneity across patients and identification of a pan-stem and progenitor gene signature for CML

(A) UMAP embedding of Lin$^-$CD34$^+$ sorted CML BM cells from nine CML patients at diagnosis (14, 274 cells across patients). Cell color indicates cluster identity after label transfer through cell projection onto an aged-matched nBM reference (the first UMAP from the left).

(B) Bar plots showing the log2 fold change in cluster distribution (%) of Lin$^-$CD34$^+$ CML BM cells (n = 9) compared to Lin$^-$CD34$^+$ from nBM. Error bars depict standard deviation.

(C) Volcano plots showing differentially expressed genes between the Lin$^-$CD34$^+$ CML clusters (across all patients, n = 9) and the corresponding clusters from nBM (adjusted p-value < .01, log2 fold change > 1/< -1). Red and black dots represent genes uniquely up- or down-regulated per cluster comparison (genes not found significantly changed in any other cluster DEG analysis). The top 10 significant, unique genes are labelled in plot. Vertical dotted lines mark a log2 fold change equal to 1 and -1.

(D) Heatmap showing the average expression of the 50 significantly up-regulated and 21 down-regulated CML signature genes (genes significantly changed and consistent through all clusters DEG analyses) across clusters from all CML patients as well as nBM (adjusted p-value < .01, log2 fold change > 1/< -1). Red indicates high expression, blue low expression.

Figure 3. Cell heterogeneity at diagnosis relates to TKI therapy outcome in CML

(A) Stacked bar plots showing the cluster distribution within Lin$^-$CD34$^+$ compartment in all CML patients at diagnosis as well as nBM. CML patients are ordered by BCR::ABL1^{IS} (%) following 12 months of TKI therapy (M12) and retrospectively stratified as per European LeukemiaNet recommendations; Optimal = CML1-4 (≤ 0.1 %), Warning = CML5-7 (> 0.1-1 %), Failure = CML8-9 (> 1 %). The total number of Lin$^-$CD34$^+$ cells from individual patients is indicated at the bottom.

(B) Box plots comparing cluster proportions in optimal responders (n = 4, CML patients 1-4) and treatment failures (n = 2, CML patients 8-9) at diagnosis; the patients were retrospectively stratified according to BCR::ABL1^{IS} (%) after 12 months of TKI therapy (Optimal ≤ 1 %), Failure > 1 %).

(C) A scheme for computational deconvolution of bulk transcriptomes from patients into constituent cell populations; using CITE-seq derived gene signatures from Lin$^-$CD34$^+$ nBM as reference, an independent bulk CD34$^+$ microarray dataset from CML patients (n = 59) (McWeeney et al., 2010) was deconvoluted into constituent cell populations using CIBERSORTx (Newman et al., 2019)

(D) Stacked bar plots showing percentage of specific clusters within CD34$^+$ cells from individual CML patients (n = 59). The x-axis shows individual GSE ID for patients, y-axis shows percentage of clusters with similar color code as used in Fig. 1-2 UMAPs. Annotation of individual patient as per the original study (McWeeney et al., 2010); non-responders with > 65 % Ph+ metaphases (did not achieve even a minor cytogenetic response), responders with 0 % Ph+ metaphases after 12 months of Imatinib therapy (achieved CCyR). BM and PB represent CD34$^+$ cells isolated from bone marrow, and peripheral blood respectively.

(E) The fold change in proportions for cell clusters between non-responders and responders (annotation as described above) for CD34$^+$ cells isolated from bone marrow; statistical significance shown by asterisk *; student t-test, p-value < .05.

Figure 4. Identification of BCR::ABL1$^+$ and BCR::ABL1$^-$ primitive cells and their surface markers by joint analysis of single cell gene expression and multiplexed antibody derived sequence tags (ADTs)

(A) Overview of analysis steps to generate Figure 4B. (1) Lin$^-$CD34$^+$CD38$^{-/low}$ cells were projected onto Lin$^-$CD34$^+$ nBM. Subsequently, the primitive cluster CITE-seq data from all CML patients and nBM (negative control) were merged and visualized together in one UMAP. BCR::ABL1$^+$ gene signatures from BCR::ABL1 targeted SMART-seq (Giustacchini et al., 2017) was used to define primitive cluster cells from the individual patients as either BCR::ABL1$^+$ or BCR::ABL1$^-$ (2) Lin$^-$CD34$^+$ and Lin$^-$CD34$^+$CD38$^{-/low}$ CITE-seq data from the same patient was merged and visualized together in a UMAP (3) BCR-ABL status from the Lin$^-$CD34$^+$CD38$^{-/low}$ primitive cells was linked to the joint UMAPs by matching cell IDs and cell were colored as either red (BCR::ABL1$^+$) or black (BCR::ABL1$^-$) (4) The log2 fold change in ADT expression between primitive Lin$^-$CD34$^+$CD38$^{-/low}$ BCR::ABL1$^+$ (red) and BCR::ABL1$^-$ (black)

cells was calculated and the remaining cells were colored according to their cluster annotation given after projection onto Lin$^-$CD34$^+$ nBM.

(B) UMAP plots showing the merged CITE-seq data of Lin$^-$CD34$^+$ and Lin$^-$CD34$^+$CD38$^{-/low}$ sorted populations for CML2-9 individually. Cells are color-coded according to cluster annotation given following projection onto Lin$^-$CD34$^+$ nBM. Lin$^-$CD34$^+$CD38$^{-/low}$ primitive cluster cells are annotated as BCR::ABL1$^+$ (red) or BCR::ABL1$^-$ (black) and display enrichment of BCR::ABL1$^+$ LSC signatures and non-leukemic stem cell signatures respectively. The red and black bars in the bar plot below indicate ADTs with significant changes in expression (p-value < .05, log2 fold change >1 / < -1) for BCR::ABL1$^+$ and BCR::ABL1$^-$ cells, respectively.

(C) Volcano plot showing differentially expressed genes between CML Lin$^-$CD34$^+$CD38$^{-/low}$ Primitive BCR::ABL1$^+$ and BCR::ABL1$^-$ cells. Red and black dots represent significant up- and down-regulated genes (adjusted p-value < .01, log2 fold change > 1/ < -1). The top 10 significant genes are labelled. Vertical dotted lines mark a fold change equal to 1 and -1.

(D) UMAP embedding of CML Lin$^-$CD34$^+$ cells from one representative CML patient at diagnosis (CML5). First plot from the left show cells colored according to the cluster identity given after mapping to nBM, the primitive cells are colored yellow. The following two UMAPs of Lin$^-$CD34$^+$ show the relative mRNA expression of the BCR::ABL1$^+$ LSC signature and BCR::ABL1$^-$ non-leukemic stem cell gene signature; scale: red = high expression, blue = low expression.

Figure 5. Assessment of surface marker combinations to capture molecularly defined BCR::ABL1$^+$ and BCR::ABL1$^-$ primitive cells

(A) Heatmap comparing ADT expression between BCR::ABL1$^+$ and BCR::ABL1$^-$ cells within the Lin$^-$CD34$^+$CD38$^{-/low}$ primitive cluster across CML patients (black = surface markers significantly up-regulated in BCR::ABL1$^-$ cells (log2 fold change < -1, p-value < .05); red = surface markers significantly up-regulated in BCR::ABL1$^+$ cells (log2 fold change > 1, p-value < .05); grey = non-significant change in ADT expression; white = surface marker was not present in the ADT panel used for the specific patient).

(B) Visualization of the relative ADT expression of CD25, CD26, CD93, CD117 and CD35 in the UMAPs of Lin$^-$CD34$^+$ cells from CML patient 5 and 9 (red = high expression, blue = low expression).

(C) Assessment of a selection of ADTs; CD25, CD26, CD93, CD117 and CD35 capacity to capture BCR::ABL1$^+$ primitive, BCR::ABL1$^-$ primitive, all primitive cells, and specific progenitors across patients by gating on their expression within the Lin$^-$CD34$^+$ compartment (x-axis shows specific clusters, y-axis: percentage of specific cluster captured; each white circle represents a patient sample).

(D) Assessment of specific ADTs: CD26, CD25 and CD35 capacity to capture BCR::ABL1^{+} primitive versus BCR::ABL1^{-} primitive cluster within the Lin^{-} CD34^{+}CD38$^{-/low}$ compartment across patients; x-axis shows specific clusters, y-axis: percentage of specific cluster captured; each white circle represents a patient sample.

(E) Assessment of specific combinations of ADTs: CD26^{+}CD35^{-}, CD26^{-}CD35^{+}, CD26^{-} CD35^{-}, and CD26^{+}CD35^{+} capacity to capture BCR::ABL1^{+} primitive versus BCR::ABL1^{-} primitive cluster within the Lin^{-}CD34^{+}CD38$^{-/low}$ compartment across patients; x-axis shows specific clusters, y-axis: percentage of specific cluster captured; each white circle represents a patient sample.

Figure 6. Analysis of CD26^{+}CD35^{-} vs. CD26^{-}CD35^{+} cells for BCR::ABL1 transcript expression, and response to TKI therapy

(A) Real time qPCR for BCR::ABL1 in CD26^{-}CD35^{+} (n = 7, CML patients 10-12, 14-15, 17-18) vs CD26^{+}CD35^{-} (n = 9, CML patients 10-15, 17-18 and 20) within the Lin^{-} CD34^{+}CD38$^{-/low}$ compartment at diagnosis and following 3 months of Bosutinib therapy (n = 3, CML patients 17, 18, 21). GAPDH served as control.

(B) Real time qPCR for GAS2 in CD26^{-}CD35^{+} (n = 3, CML patients 14, 17-18) vs CD26^{+}CD35^{-} (n = 4, CML patients 13-14, 17-18) within the Lin^{-}CD34^{+}CD38$^{-/low}$ compartment at diagnosis and following 3 months of Bosutinib therapy (n = 3, CML patients 17-18, 21). GAPDH served as control.

(C) Representative FACS plots showing the percentage CD26^{+}CD35^{-} (LSC) and CD26^{-} CD35^{+} (HSC) cells within the Lin^{-}CD34^{+}CD38$^{-/low}$ compartment. Left panel: ADT gated CD26^{+}CD35^{-} and CD26^{-}CD35^{+} cells within Lin^{-}CD34^{+}CD38$^{-/low}$ CITE-seq data from selected optimal responder (CML4) and treatment failure (CML8) at diagnosis. Right panel: FACS gated Lin^{-}CD34^{+}CD38$^{-/low}$CD26^{+}CD35^{-} and CD26^{-}CD35^{+} cells in selected optimal responder (CML12) and treatment failure (CML13) at diagnosis versus 3 months of TKI therapy (Bosutinib).

(D) Bar plots showing the percentage of CD26^{+}CD35^{-} and CD26^{-}CD35^{+} cells within Lin^{-}CD34^{+}CD38$^{-/low}$ compartment from optimal responders and treatment failures at diagnosis (n = 11; optimal = 6 (≤ 0.1 %, CML patients 12, 14-18), failure = 5 (> 1 %, CML patients 13, 19, 22-23, 25) and following 3 months of Bosutinib therapy (n = 11; optimal = 6 (≤ 0.1 %, CML patients 12, 14-18), failure = 5 (> 1 %, CML patients 13, 19, 22-23, 24) determined using FACS.

Supplementary Figures

Supplementary Figure 1.

(A) Distribution of annotated cell clusters across the two Lin-CD34+ nBM samples.

(B) Cell cycle scoring: G1, S, G2/M of UMAP embedded Lin-CD34+ cells from nBM using Scarf.

(C) Visualization of the relative mRNA (left panels) and ADT expression (right panels) of a selection of genes and surface markers within the Lin-CD34+ nBM reference.

Supplementary Figure 2.

(A) UMAP plots showing the mapping score for the individual Lin$^-$CD34$^+$ CML samples at diagnosis when mapped onto the nBM reference; mapping was performed using Scarf (Dhapola et al., 2022). Circle size indicates mapping score and circle color specify cluster identity of the reference cell.

(B) Bar plots showing the log2 fold change in cluster distribution (%) within the CML Lin$^-$CD34$^+$ compartment at diagnosis when compared to nBM for the individual CML patients.

Supplementary Figure 3.

(A) Volcano plots showing differentially expressed genes between Lin$^-$CD34$^+$ CML (n = 9) at diagnosis and nBM cells across clusters (DESeq2). Red and black dots represent genes found to be consistently significant up- or down-regulated across all cluster comparisons in CML, respectively (adjusted p-value < .01, log2 fold change = >1 / < -1). Vertical dotted line marks a log2 fold change equal to 1 and -1.

(B) The fold change in proportions for cell clusters between all non-responders and responders (CD34$^+$ cells isolated from both PB and BM); statistical significance shown by asterisk *; student t-test, p-value < .05.

(C) Assessment of the CML related ADTs; CD25, CD26, CD93 capacity to capture primitive cells, and specific progenitors across patients by gating on their expression within the Lin$^-$CD34$^+$ compartment (x-axis shows specific clusters, y-axis: percentage of specific cluster captured; each white circle represents a patient sample).

Supplementary figure 4.

(A) UMAP plots showing the mapping score for individual Lin$^-$CD34$^+$CD38$^{-/low}$ CML samples (CML2-8) at diagnosis and Lin$^-$CD34$^+$CD38$^{-/low}$ normal BM when mapped onto the Lin$^-$CD34$^+$ nBM reference; mapping was performed using Scarf. Circle size indicates mapping score and circle color specify cluster identity of the reference cell.

(B) UMAP embedding of Lin$^-$CD34$^+$CD38$^{-/low}$ primitive cluster CML (n = 8, a total of 2778 cells) and normal BM cells showing clusters following Leiden clustering analysis.

(C) UMAP embedding of Lin$^-$CD34$^+$CD38$^{-/low}$ primitive cluster CML (n = 8, a total of 2778 cells) at diagnosis and normal BM cells where cells are colored by sample identity.

(D) Same UMAP as in B-C above, showing the relative expression of BCR::ABL1$^+$ LSC (left panel) and BCR::ABL1$^-$ LSC signature genes (right panel) used to define BCR::ABL1$^+$ primitive cells (Signature genes are from DEG analysis comparing CP-CML Lin$^-$CD34$^+$CD38$^{-/low}$ BCR::ABL1$^+$ and BCR::ABL1$^-$ (Giustacchini et al., 2017)).

(E) Same UMAP as in B-C above, showing the relative expression of BCR::ABL1$^+$ LSC (left panel) and nBM HSC signature genes (right panel) used to define BCR::ABL1$^+$ primitive cells (Signature genes are from DEG analysis comparing CP-CML Lin$^-$CD34$^+$CD38$^{-/low}$ BCR::ABL1$^+$ and nBM Lin$^-$CD34$^+$CD38$^{-/low}$ cells (Giustacchini et al., 2017)).

(F) Quantification of Lin$^-$CD34$^+$CD38$^{-/low}$ primitive BCR::ABL1$^+$ (red) and BCR::ABL1$^-$ (black) cells per CML patient at diagnosis. Total primitive cells per patient is indicated at the bottom.

Supplementary figure 5.

(A) UMAP plots where CITE-seq data from Lin$^-$CD34$^+$ and Lin$^-$CD34$^+$CD38$^{-/low}$ sorted cells from the same CML patients have been merged, and Lin$^-$CD34$^+$CD38$^{-/low}$ cells are highlighted in blue.

(B) UMAP plots where CITE-seq data from Lin$^-$CD34$^+$ and Lin$^-$CD34$^+$CD38$^{-/low}$ sorted cells from the same CML patients have been merged, where Lin$^-$CD34$^+$CD38$^{-/low}$ primitive annotated cells are highlighted in blue.

Supplementary figure 6.

(A) UMAP plots of Lin$^-$CD34$^+$ cells from CML patients 1-4 and 6-9, showing cells colored according to cluster identity given after mapping to nBM (left panel); the relative expression of Lin$^-$CD34$^+$CD38$^{-/low}$ Primitive BCR::ABL1$^+$ signature genes (center panel) and the relative expression of Lin$^-$CD34$^+$CD38$^{-/low}$ Primitive BCR::ABL1$^-$ signature genes (right panel). DEG analysis is shown in Figure 4C and relative expression of signatures for CML5 is found in Figure 4D. (red = high expression, blue = low expression).

Supplementary figure 7.

(A) UMAP plots of CML Lin$^-$CD34$^+$ primitive cluster cells from all CML patients (n = 9, a total of 1 106 cells) showing clusters following Leiden clustering analysis.

(B) UMAP plots of CML Lin$^-$CD34$^+$ primitive cluster from all CML patients (n = 9, a total of 1 106 cells) where the cells are colored as per the sample identity

(C) UMAP plots of CML Lin$^-$CD34$^+$ primitive cluster cells from all CML patients showing the relative expression of two DEG signatures used to define BCR::ABL1$^+$ primitive cells: (1) BCR::ABL1$^+$ LSC vs nBM HSC signature genes (top row, left panel = up-regulated genes in BCR::ABL1$^+$ LSCs, right panel = genes up-regulated in nBM HSCs), (2) BCR::ABL1$^+$ LSC vs BCR::ABL1$^-$ LSC (bottom row, left panel = genes

up-regulated in BCR::ABL1^{+} LSC, right panel = genes up-regulated in BCR::ABL1^{-} LSC) (Giustacchini et al., 2017).

(D) UMAP plots of Lin^{-}CD34^{+} cells from individual CML patients (1-9) showing primitive cluster cells (yellow cluster, left panel) annotated as BCR::ABL1^{+} (red) and BCR::ABL1^{-} (black)(right panel).

(E) Quantification of Lin^{-}CD34^{+} primitive BCR::ABL1^{+} (red, cluster 2-3 Supp. Fig. 7A) and BCR::ABL1^{-} (black, cluster 1 Supp. Fig. 7A) cells per CML patient at diagnosis. Total primitive cells are indicated at the bottom.

Supplementary figure 8.

(A) UMAP plots of Lin^{-}CD34^{+} cells from CML patients 1-4 and 6-8 showing the relative ADT expression of a selection of markers (CD25, CD26, CD93, CD117, CD35) (red = high expression, blue = low expression). ADT expression for CML patient 5 and 9 is shown in Fig. 5B.

Supplementary figure 9.

(A) Plots showing representative gates on ADT expression for CD26, CD35, CD117, CD25, CD93 within the Lin^{-}CD34^{+} CITE-seq data using FlowJo. Gates are shown for CML5 and CML9.

(B) Plots showing the gating on CD26 and CD35 ADT expression within the Lin^{-}CD34^{+}CD38$^{-/low}$ CITE-seq data for CML patients 2-3, 5-7 and 9 using FlowJo. Plots for CML patient 4 and 8 is shown in Fig. 6D.

(C) Cumulative plots of time to first division kinetics from Lin^{-}CD34^{+}CD38$^{-/low}$CD45RA^{-}CD26^{+}CD35^{-} and CD26^{-}CD35^{+} single cells for two individual CML patients at diagnosis (n = 2, CML patients 10 and 11). Dead cells and non-dividing cells were excluded from the analysis.

(D) Mean time to first division (hours) for Lin^{-}CD34^{+}CD38$^{-/low}$CD45RA^{-} CD26^{+}CD35^{-} or CD26^{-}CD35^{+} single cells from the two CML patients shown in C (n = 2, CML patients 10 and 11) (p-value = ns., .84; paired t-test).

(E) Mean cell cycle status of ADT gated CD26^{+}CD35^{-} or CD26^{-}CD35^{+} cells, after running Scarf's cell cycle scoring on the Lin^{-}CD34^{+}CD38$^{-/low}$ CITE-seq data for patients individually (n = 8, CML2-9).

(F) Mean cell cycle status of ADT gated CD26^{+}CD35^{-} or CD26^{-}CD35^{+} cells, after running Scarf's cell cycle scoring on Lin^{-}CD34^{+}CD38$^{-/low}$ Primitive cluster for patients individually (n = 8, CML2-9).

Supplementary tables

Supplementary Table 1

CML sample cohort

Supplementary Table 2

CITE-seq antibodies

Supplementary Table 3

FACS antibodies

Supplementary Table 4

List of marker genes for nBM clusters

Supplementary Table 5

List of DEG uniquely changed per cluster in CML vs. nBM clusters 1-11 along with their fold change.

Supplementary Table 6

List of DEG up- and down-regulated in all clusters in CML vs. nBM clusters 1-11.

Supplementary Table 7

Lits of DEG along with their fold change between BCR::ABL1^{+} LSCs versus BCR::ABL1^{-} stem cells.

References

Barbieri, D. A., Telonis, A. G., & Figueroa, M. K. E. (2022). Corticotropin Releasing Hormone Binding Protein (CRHBP) Regulates Hematopoietic Function and Acts As a Novel AML Tumor Suppressor through a Crh-Independent Mechanism. *Blood*, *140*, 5840-5841. https://doi.org/10.1182/blood-2022-159719

Baryawno, N., Severe, N., & Scadden, D. T. (2017). Hematopoiesis: Reconciling Historic Controversies about the Niche. *Cell Stem Cell*, *20*(5), 590-592. https://doi.org/10.1016/j.stem.2017.03.025

Bergamaschi, G., Podesta, M., Frassoni, F., Rosti, V., Carella, A. M., Saglio, G., & Cazzola, M. (1994). Restoration of normal polyclonal haemopoiesis in patients with chronic myeloid leukaemia autografted with Ph-negative peripheral stem cells. *Br J Haematol*, *87*(4), 867-870. https://doi.org/10.1111/j.1365-2141.1994.tb06755.x

Bhatia, R., Holtz, M., Niu, N., Gray, R., Snyder, D. S., Sawyers, C. L., Arber, D. A., Slovak, M. L., & Forman, S. J. (2003). Persistence of malignant hematopoietic progenitors in chronic myelogenous leukemia patients in complete cytogenetic remission following imatinib mesylate treatment. *Blood*, *101*(12), 4701-4707. https://doi.org/10.1182/blood-2002-09-2780

Bolton-Gillespie, E., Schemionek, M., Klein, H. U., Flis, S., Hoser, G., Lange, T., Nieborowska-Skorska, M., Maier, J., Kerstiens, L., Koptyra, M., Muller, M. C., Modi, H., Stoklosa, T., Seferynska, I., Bhatia, R., Holyoake, T. L., Koschmieder, S., &

Skorski, T. (2013). Genomic instability may originate from imatinib-refractory chronic myeloid leukemia stem cells. *Blood*, *121*(20), 4175-4183. https://doi.org/10.1182/blood-2012-11-466938

Branford, S., Kim, D. D. H., Apperley, J. F., Eide, C. A., Mustjoki, S., Ong, S. T., Nteliopoulos, G., Ernst, T., Chuah, C., Gambacorti-Passerini, C., Mauro, M. J., Druker, B. J., Kim, D. W., Mahon, F. X., Cortes, J., Radich, J. P., Hochhaus, A., Hughes, T. P., & International, C. M. L. F. G. A. (2019). Laying the foundation for genomically-based risk assessment in chronic myeloid leukemia. *Leukemia*, *33*(8), 1835-1850. https://doi.org/10.1038/s41375-019-0512-y

Braun, T. P., Eide, C. A., & Druker, B. J. (2020). Response and Resistance to BCR-ABL1-Targeted Therapies. *Cancer Cell*, *37*(4), 530-542. https://doi.org/10.1016/j.ccell.2020.03.006

Carella, A. M., Pollicardo, N., Pungolino, E., Raffo, M. R., Podesta, M., Ferrero, R., Pierluigi, D., Nati, S., Naibo, K., Congiu, A., & et al. (1993). Mobilization of cytogenetically 'normal' blood progenitors cells by intensive conventional chemotherapy for chronic myeloid and acute lymphoblastic leukemia. *Leuk Lymphoma*, *9*(6), 477-483. https://doi.org/10.3109/10428199309145754

Chen, Y., Mobius, S., Riege, K., Hoffmann, S., Hochhaus, A., Ernst, T., & Rudolph, K. L. (2023). Genetic separation of chronic myeloid leukemia stem cells from normal hematopoietic stem cells at single-cell resolution. *Leukemia*. https://doi.org/10.1038/s41375-023-01929-6

Claxton, D., Deisseroth, A., Talpaz, M., Reading, C., Kantarjian, H., Trujillo, J., Stass, S., Gooch, G., & Spitzer, G. (1992). Polyclonal hematopoiesis in interferon-induced cytogenetic remissions of chronic myelogenous leukemia. *Blood*, *79*(4), 997-1002. https://www.ncbi.nlm.nih.gov/pubmed/1371081

Corbin, A. S., Agarwal, A., Loriaux, M., Cortes, J., Deininger, M. W., & Druker, B. J. (2011). Human chronic myeloid leukemia stem cells are insensitive to imatinib despite inhibition of BCR-ABL activity. *J Clin Invest*, *121*(1), 396-409. https://doi.org/10.1172/JCI35721

Cortes, J., Pavlovsky, C., & Saussele, S. (2021). Chronic myeloid leukaemia. *Lancet*, *398*(10314), 1914-1926. https://doi.org/10.1016/S0140-6736(21)01204-6

Coulombel, L., Kalousek, D. K., Eaves, C. J., Gupta, C. M., & Eaves, A. C. (1983). Long-term marrow culture reveals chromosomally normal hematopoietic progenitor cells in patients with Philadelphia chromosome-positive chronic myelogenous leukemia. *N Engl J Med*, *308*(25), 1493-1498. https://doi.org/10.1056/NEJM198306233082502

Deininger, M. W. (2003). Cytogenetic studies in patients on imatinib. *Semin Hematol*, *40*(2 Suppl 2), 50-55. https://doi.org/10.1053/shem.2003.50043

Dhapola, P., Rodhe, J., Olofzon, R., Bonald, T., Erlandsson, E., Soneji, S., & Karlsson, G. (2022). Scarf enables a highly memory-efficient analysis of large-scale single-cell genomics data. *Nat Commun*, *13*(1), 4616. https://doi.org/10.1038/s41467-022-32097-3

Eisterer, W., Jiang, X., Christ, O., Glimm, H., Lee, K. H., Pang, E., Lambie, K., Shaw, G., Holyoake, T. L., Petzer, A. L., Auewarakul, C., Barnett, M. J., Eaves, C. J., & Eaves, A. C. (2005). Different subsets of primary chronic myeloid leukemia stem cells engraft immunodeficient mice and produce a model of the human disease. *Leukemia*, *19*(3), 435-441. https://doi.org/10.1038/sj.leu.2403649

Fathy El-Metwaly, N., Aref, S., Ayed, M., Abdel Hamid, M., & El-Sokkary, A. M. A. (2021). CD34+/CD38- Stem Cell Burden Could Predict Chronic Myeloid Leukemia Patients' Outcome. *Asian Pac J Cancer Prev*, *22*(10), 3237-3243. https://doi.org/10.31557/APJCP.2021.22.10.3237

Giustacchini, A., Thongjuea, S., Barkas, N., Woll, P. S., Povinelli, B. J., Booth, C. A. G., Sopp, P., Norfo, R., Rodriguez-Meira, A., Ashley, N., Jamieson, L., Vyas, P., Anderson, K., Segerstolpe, A., Qian, H., Olsson-Stromberg, U., Mustjoki, S., Sandberg, R., Jacobsen, S. E. W., & Mead, A. J. (2017). Single-cell transcriptomics uncovers distinct molecular

signatures of stem cells in chronic myeloid leukemia. *Nat Med*, *23*(6), 692-702. https://doi.org/10.1038/nm.4336

Gullaksen, S. E., Bader, L., Hellesoy, M., Sulen, A., Fagerholt, O. H. E., Engen, C. B., Skavland, J., Gjertsen, B. T., & Gavasso, S. (2019). Titrating Complex Mass Cytometry Panels. *Cytometry A*, *95*(7), 792-796. https://doi.org/10.1002/cyto.a.23751

Haas, S., Trumpp, A., & Milsom, M. D. (2018). Causes and Consequences of Hematopoietic Stem Cell Heterogeneity. *Cell Stem Cell*, *22*(5), 627-638. https://doi.org/10.1016/j.stem.2018.04.003

Hamilton, A., Helgason, G. V., Schemionek, M., Zhang, B., Myssina, S., Allan, E. K., Nicolini, F. E., Muller-Tidow, C., Bhatia, R., Brunton, V. G., Koschmieder, S., & Holyoake, T. L. (2012). Chronic myeloid leukemia stem cells are not dependent on Bcr-Abl kinase activity for their survival. *Blood*, *119*(6), 1501-1510. https://doi.org/10.1182/blood-2010-12-326843

He, X., Gonzalez, V., Tsang, A., Thompson, J., Tsang, T. C., & Harris, D. T. (2005). Differential gene expression profiling of CD34+ CD133+ umbilical cord blood hematopoietic stem progenitor cells. *Stem Cells Dev*, *14*(2), 188-198. https://doi.org/10.1089/scd.2005.14.188

Herrmann, H., Sadovnik, I., Cerny-Reiterer, S., Rulicke, T., Stefanzl, G., Willmann, M., Hoermann, G., Bilban, M., Blatt, K., Herndlhofer, S., Mayerhofer, M., Streubel, B., Sperr, W. R., Holyoake, T. L., Mannhalter, C., & Valent, P. (2014). Dipeptidylpeptidase IV (CD26) defines leukemic stem cells (LSC) in chronic myeloid leukemia. *Blood*, *123*(25), 3951-3962. https://doi.org/10.1182/blood-2013-10-536078

Hochhaus, A., Baccarani, M., Silver, R. T., Schiffer, C., Apperley, J. F., Cervantes, F., Clark, R. E., Cortes, J. E., Deininger, M. W., Guilhot, F., Hjorth-Hansen, H., Hughes, T. P., Janssen, J., Kantarjian, H. M., Kim, D. W., Larson, R. A., Lipton, J. H., Mahon, F. X., Mayer, J., . . . Hehlmann, R. (2020). European LeukemiaNet 2020 recommendations for treating chronic myeloid leukemia. *Leukemia*, *34*(4), 966-984. https://doi.org/10.1038/s41375-020-0776-2

Holyoake, T. L., & Vetrie, D. (2017). The chronic myeloid leukemia stem cell: stemming the tide of persistence. *Blood*, *129*(12), 1595-1606. https://doi.org/10.1182/blood-2016-09-696013

Hsieh, Y. C., Kirschner, K., & Copland, M. (2021). Improving outcomes in chronic myeloid leukemia through harnessing the immunological landscape. *Leukemia*, *35*(5), 1229-1242. https://doi.org/10.1038/s41375-021-01238-w

Husmann, D., & Gozani, O. (2019). Histone lysine methyltransferases in biology and disease. *Nat Struct Mol Biol*, *26*(10), 880-889. https://doi.org/10.1038/s41594-019-0298-7

Irizarry, R. A., Hobbs, B., Collin, F., Beazer-Barclay, Y. D., Antonellis, K. J., Scherf, U., & Speed, T. P. (2003). Exploration, normalization, and summaries of high density oligonucleotide array probe level data. *Biostatistics*, *4*(2), 249-264. https://doi.org/10.1093/biostatistics/4.2.249

Janssen, J. J., Deenik, W., Smolders, K. G., van Kuijk, B. J., Pouwels, W., Kelder, A., Cornelissen, J. J., Schuurhuis, G. J., & Ossenkoppele, G. J. (2012). Residual normal stem cells can be detected in newly diagnosed chronic myeloid leukemia patients by a new flow cytometric approach and predict for optimal response to imatinib. *Leukemia*, *26*(5), 977-984. https://doi.org/10.1038/leu.2011.347

Janssen, J. J., Klaver, S. M., Waisfisz, Q., Pasterkamp, G., de Kleijn, D. P., Schuurhuis, G. J., & Ossenkoppele, G. J. (2005). Identification of genes potentially involved in disease transformation of CML. *Leukemia*, *19*(6), 998-1004. https://doi.org/10.1038/sj.leu.2403735

Jaras, M., Johnels, P., Hansen, N., Agerstam, H., Tsapogas, P., Rissler, M., Lassen, C., Olofsson, T., Bjerrum, O. W., Richter, J., & Fioretos, T. (2010). Isolation and killing of candidate chronic myeloid leukemia stem cells by antibody targeting of IL-1 receptor accessory protein. *Proc Natl Acad Sci U S A*, *107*(37), 16280-16285. https://doi.org/10.1073/pnas.1004408107

Kaeser, M. D., Aslanian, A., Dong, M. Q., Yates, J. R., 3rd, & Emerson, B. M. (2008). BRD7, a novel PBAF-specific SWI/SNF subunit, is required for target gene activation and repression in embryonic stem cells. *J Biol Chem*, *283*(47), 32254-32263. https://doi.org/10.1074/jbc.M806061200

Kar, A., Saha, D., Purohit, G., Singh, A., Kumar, P., Yadav, V. K., Kumar, P., Thakur, R. K., & Chowdhury, S. (2012). Metastases suppressor NME2 associates with telomere ends and telomerase and reduces telomerase activity within cells. *Nucleic Acids Res*, *40*(6), 2554-2565. https://doi.org/10.1093/nar/gkr1109

Khorashad, J. S., Anand, M., Marin, D., Saunders, S., Al-Jabary, T., Iqbal, A., Margerison, S., Melo, J. V., Goldman, J. M., Apperley, J. F., & Kaeda, J. (2006). The presence of a BCR-ABL mutant allele in CML does not always explain clinical resistance to imatinib. *Leukemia*, *20*(4), 658-663. https://doi.org/10.1038/sj.leu.2404137

Kinstrie, R., Horne, G. A., Morrison, H., Irvine, D., Munje, C., Castaneda, E. G., Moka, H. A., Dunn, K., Cassels, J. E., Parry, N., Clarke, C. J., Scott, M. T., Clark, R. E., Holyoake, T. L., Wheadon, H., & Copland, M. (2020). CD93 is expressed on chronic myeloid leukemia stem cells and identifies a quiescent population which persists after tyrosine kinase inhibitor therapy. *Leukemia*, *34*(6), 1613-1625. https://doi.org/10.1038/s41375-019-0684-5

Krishnan, V., Schmidt, F., Nawaz, Z., Venkatesh, P. N., Lee, K. L., Ren, X., Chan, Z. E., Yu, M., Makheja, M., Rayan, N. A., Lim, M. G. L., Cheung, A. M. S., Bari, S., Chng, W. J., Than, H., Ouyang, J., Rackham, O., Tan, T. Z., Hwang, W. Y. K., . . . Ong, S. T. (2023). A single-cell atlas identifies pretreatment features of primary imatinib resistance in chronic myeloid leukemia. *Blood*, *141*(22), 2738-2755. https://doi.org/10.1182/blood.2022017295

Landberg, N., von Palffy, S., Askmyr, M., Lilljebjorn, H., Sanden, C., Rissler, M., Mustjoki, S., Hjorth-Hansen, H., Richter, J., Agerstam, H., Jaras, M., & Fioretos, T. (2018). CD36 defines primitive chronic myeloid leukemia cells less responsive to imatinib but vulnerable to antibody-based therapeutic targeting. *Haematologica*, *103*(3), 447-455. https://doi.org/10.3324/haematol.2017.169946

Lenaerts, T., Pacheco, J. M., Traulsen, A., & Dingli, D. (2010). Tyrosine kinase inhibitor therapy can cure chronic myeloid leukemia without hitting leukemic stem cells. *Haematologica*, *95*(6), 900-907. https://doi.org/10.3324/haematol.2009.015271

Lipton, J. H., Brummendorf, T. H., Gambacorti-Passerini, C., Garcia-Gutierrez, V., Deininger, M. W., & Cortes, J. E. (2022). Long-term safety review of tyrosine kinase inhibitors in chronic myeloid leukemia - What to look for when treatment-free remission is not an option. *Blood Rev*, *56*, 100968. https://doi.org/10.1016/j.blre.2022.100968

Marjanovic, N. D., Weinberg, R. A., & Chaffer, C. L. (2013). Cell plasticity and heterogeneity in cancer. *Clin Chem*, *59*(1), 168-179. https://doi.org/10.1373/clinchem.2012.184655

McWeeney, S. K., Pemberton, L. C., Loriaux, M. M., Vartanian, K., Willis, S. G., Yochum, G., Wilmot, B., Turpaz, Y., Pillai, R., Druker, B. J., Snead, J. L., MacPartlin, M., O'Brien, S. G., Melo, J. V., Lange, T., Harrington, C. A., & Deininger, M. W. (2010). A gene expression signature of CD34+ cells to predict major cytogenetic response in chronic-phase chronic myeloid leukemia patients treated with imatinib. *Blood*, *115*(2), 315-325. https://doi.org/10.1182/blood-2009-03-210732

Michor, F., Hughes, T. P., Iwasa, Y., Branford, S., Shah, N. P., Sawyers, C. L., & Nowak, M. A. (2005). Dynamics of chronic myeloid leukaemia. *Nature*, *435*(7046), 1267-1270. https://doi.org/10.1038/nature03669

Mustjoki, S., Richter, J., Barbany, G., Ehrencrona, H., Fioretos, T., Gedde-Dahl, T., Gjertsen, B. T., Hovland, R., Hernesniemi, S., Josefsen, D., Koskenvesa, P., Dybedal, I., Markevarn, B., Olofsson, T., Olsson-Stromberg, U., Rapakko, K., Thunberg, S., Stenke, L., Simonsson, B., . . . Nordic, C. M. L. S. G. (2013). Impact of malignant stem cell burden on therapy outcome in newly diagnosed chronic myeloid leukemia patients. *Leukemia*, *27*(7), 1520-1526. https://doi.org/10.1038/leu.2013.19

Newman, A. M., Steen, C. B., Liu, C. L., Gentles, A. J., Chaudhuri, A. A., Scherer, F., Khodadoust, M. S., Esfahani, M. S., Luca, B. A., Steiner, D., Diehn, M., & Alizadeh,

A. A. (2019). Determining cell type abundance and expression from bulk tissues with digital cytometry. *Nat Biotechnol*, *37*(7), 773-782. https://doi.org/10.1038/s41587-019-0114-2

Nieborowska-Skorska, M., Kopinski, P. K., Ray, R., Hoser, G., Ngaba, D., Flis, S., Cramer, K., Reddy, M. M., Koptyra, M., Penserga, T., Glodkowska-Mrowka, E., Bolton, E., Holyoake, T. L., Eaves, C. J., Cerny-Reiterer, S., Valent, P., Hochhaus, A., Hughes, T. P., van der Kuip, H., . . . Skorski, T. (2012). Rac2-MRC-cIII-generated ROS cause genomic instability in chronic myeloid leukemia stem cells and primitive progenitors. *Blood*, *119*(18), 4253-4263. https://doi.org/10.1182/blood-2011-10-385658

O'Hare, T., Eide, C. A., & Deininger, M. W. (2007). Bcr-Abl kinase domain mutations, drug resistance, and the road to a cure for chronic myeloid leukemia. *Blood*, *110*(7), 2242-2249. https://doi.org/10.1182/blood-2007-03-066936

Pacelli, P., Santoni, A., Sicuranza, A., Abruzzese, E., Giai, V., Crugnola, M., Annunziata, M., Galimberti, S., Iurlo, A., Luciano, L., Sora, F., Fava, C., Bestoso, E., Marzano, C., Cartocci, A., Defina, M., Sammartano, V., Cencini, E., Raspadori, D., & Bocchia, M. (2023). Prospective monitoring of chronic myeloid leukemia patients from the time of TKI discontinuation: the fate of peripheral blood CD26(+) leukemia stem cells. *Front Pharmacol*, *14*, 1194712. https://doi.org/10.3389/fphar.2023.1194712

Pagani, I. S., Dang, P., Saunders, V. A., Grose, R., Shanmuganathan, N., Kok, C. H., Carne, L., Rwodzi, Z., Watts, S., McLean, J., Braley, J., Altamura, H., Yeung, D. T., Branford, S., Yong, A. S. M., White, D. L., Hughes, T. P., & Ross, D. M. (2020). Lineage of measurable residual disease in patients with chronic myeloid leukemia in treatment-free remission. *Leukemia*, *34*(4), 1052-1061. https://doi.org/10.1038/s41375-019-0647-x

Patel, S. B., Kuznetsova, V., Matkins, V. R., Franceski, A. M., Bassal, M. A., & Welner, R. S. (2022). Ex Vivo Expansion of Phenotypic and Transcriptomic Chronic Myeloid Leukemia Stem Cells. *Exp Hematol*, *115*, 1-13. https://doi.org/10.1016/j.exphem.2022.09.001

Pellin, D., Loperfido, M., Baricordi, C., Wolock, S. L., Montepeloso, A., Weinberg, O. K., Biffi, A., Klein, A. M., & Biasco, L. (2019). A comprehensive single cell transcriptional landscape of human hematopoietic progenitors. *Nat Commun*, *10*(1), 2395. https://doi.org/10.1038/s41467-019-10291-0

Petzer, A. L., Eaves, C. J., Lansdorp, P. M., Ponchio, L., Barnett, M. J., & Eaves, A. C. (1996). Characterization of primitive subpopulations of normal and leukemic cells present in the blood of patients with newly diagnosed as well as established chronic myeloid leukemia. *Blood*, *88*(6), 2162-2171. https://www.ncbi.nlm.nih.gov/pubmed/8822936

Quagliano, A., Gopalakrishnapillai, A., Kolb, E. A., & Barwe, S. P. (2020). CD81 knockout promotes chemosensitivity and disrupts in vivo homing and engraftment in acute lymphoblastic leukemia. *Blood Adv*, *4*(18), 4393-4405. https://doi.org/10.1182/bloodadvances.2020001592

Radich, J., Yeung, C., & Wu, D. (2019). New approaches to molecular monitoring in CML (and other diseases). *Blood*, *134*(19), 1578-1584. https://doi.org/10.1182/blood.2019000838

Radich, J. P., Dai, H., Mao, M., Oehler, V., Schelter, J., Druker, B., Sawyers, C., Shah, N., Stock, W., Willman, C. L., Friend, S., & Linsley, P. S. (2006). Gene expression changes associated with progression and response in chronic myeloid leukemia. *Proc Natl Acad Sci U S A*, *103*(8), 2794-2799. https://doi.org/10.1073/pnas.0510423103

Radich, J. P., Wall, M., Branford, S., Campbell, C. D., Chaturvedi, S., DeAngelo, D. J., Deininger, M., Guinney, J., Hochhaus, A., Hughes, T. P., Kantarjian, H. M., Larson, R. A., Li, S., Maegawa, R., Mishra, K., Obourn, V., Pinilla-Ibarz, J., Purkayastha, D., Sadek, I., . . . Druker, B. J. (2023). Molecular response in newly diagnosed chronic-phase chronic myeloid leukemia: prediction modeling and pathway analysis. *Haematologica*, *108*(6), 1567-1578. https://doi.org/10.3324/haematol.2022.281878

Sadovnik, I., Hoelbl-Kovacic, A., Herrmann, H., Eisenwort, G., Cerny-Reiterer, S., Warsch, W., Hoermann, G., Greiner, G., Blatt, K., Peter, B., Stefanzl, G., Berger, D., Bilban,

M., Herndlhofer, S., Sill, H., Sperr, W. R., Streubel, B., Mannhalter, C., Holyoake, T. L., . . . Valent, P. (2016). Identification of CD25 as STAT5-Dependent Growth Regulator of Leukemic Stem Cells in Ph+ CML. *Clin Cancer Res*, *22*(8), 2051-2061. https://doi.org/10.1158/1078-0432.CCR-15-0767

Safi, F., Dhapola, P., Warsi, S., Sommarin, M., Erlandsson, E., Ungerback, J., Warfvinge, R., Sitnicka, E., Bryder, D., Boiers, C., Thakur, R. K., & Karlsson, G. (2022). Concurrent stem- and lineage-affiliated chromatin programs precede hematopoietic lineage restriction. *Cell Rep*, *39*(6), 110798. https://doi.org/10.1016/j.celrep.2022.110798

Shah, M., Kumar, H., Qiu, S., Li, H., Harris, M., He, J., Abraham, A., Crossman, D. K., Paterson, A., Welner, R. S., & Bhatia, R. (2023). Low c-Kit expression identifies primitive, therapy-resistant CML stem cells. *JCI Insight*, *8*(1). https://doi.org/10.1172/jci.insight.157421

Sommarin, M. N. E., Dhapola, P., Safi, F., Warfvinge, R., Ulfsson, L. G., Erlandsson, E., Konturek-Ciesla, A., Thakur, R. K., Böiers, C., Bryder, D., & Karlsson, G. (2021). Single-Cell Multiomics Reveals Distinct Cell States at the Top of Human Hematopoietic Hierarchy. *bioRxiv*, 2021.2004.2001.437998. https://doi.org/10.1101/2021.04.01.437998

Sorel, N., Bonnet, M. L., Guillier, M., Guilhot, F., Brizard, A., & Turhan, A. G. (2004). Evidence of ABL-kinase domain mutations in highly purified primitive stem cell populations of patients with chronic myelogenous leukemia. *Biochem Biophys Res Commun*, *323*(3), 728-730. https://doi.org/10.1016/j.bbrc.2004.08.169

Stoeckius, M., Hafemeister, C., Stephenson, W., Houck-Loomis, B., Chattopadhyay, P. K., Swerdlow, H., Satija, R., & Smibert, P. (2017). Simultaneous epitope and transcriptome measurement in single cells. *Nat Methods*, *14*(9), 865-868. https://doi.org/10.1038/nmeth.4380

Sugiyama, T., Kohara, H., Noda, M., & Nagasawa, T. (2006). Maintenance of the hematopoietic stem cell pool by CXCL12-CXCR4 chemokine signaling in bone marrow stromal cell niches. *Immunity*, *25*(6), 977-988. https://doi.org/10.1016/j.immuni.2006.10.016

Thakur, R. K., Kumar, P., Halder, K., Verma, A., Kar, A., Parent, J. L., Basundra, R., Kumar, A., & Chowdhury, S. (2009). Metastases suppressor NM23-H2 interaction with G-quadruplex DNA within c-MYC promoter nuclease hypersensitive element induces c-MYC expression. *Nucleic Acids Res*, *37*(1), 172-183. https://doi.org/10.1093/nar/gkn919

Thakur, R. K., Yadav, V. K., Kumar, A., Singh, A., Pal, K., Hoeppner, L., Saha, D., Purohit, G., Basundra, R., Kar, A., Halder, R., Kumar, P., Baral, A., Kumar, M. J., Baldi, A., Vincenzi, B., Lorenzon, L., Banerjee, R., Kumar, P., . . . Chowdhury, S. (2014). Non-metastatic 2 (NME2)-mediated suppression of lung cancer metastasis involves transcriptional regulation of key cell adhesion factor vinculin. *Nucleic Acids Res*, *42*(18), 11589-11600. https://doi.org/10.1093/nar/gku860

Thakur, R. K., Yadav, V. K., Kumar, P., & Chowdhury, S. (2011). Mechanisms of non-metastatic 2 (NME2)-mediated control of metastasis across tumor types. *Naunyn Schmiedebergs Arch Pharmacol*, *384*(4-5), 397-406. https://doi.org/10.1007/s00210-011-0631-0

Thielen, N., Richter, J., Baldauf, M., Barbany, G., Fioretos, T., Giles, F., Gjertsen, B. T., Hochhaus, A., Schuurhuis, G. J., Sopper, S., Stenke, L., Thunberg, S., Wolf, D., Ossenkoppele, G., Porkka, K., Janssen, J., & Mustjoki, S. (2016). Leukemic Stem Cell Quantification in Newly Diagnosed Patients With Chronic Myeloid Leukemia Predicts Response to Nilotinib Therapy. *Clin Cancer Res*, *22*(16), 4030-4038. https://doi.org/10.1158/1078-0432.CCR-15-2791

Tschiedel, S., Bach, E., Jilo, A., Wang, S. Y., Lange, T., Al-Ali, H. K., Vucinic, V., Niederwieser, D., & Cross, M. (2012). Bcr-Abl dependent post-transcriptional activation of NME2 expression is a specific and common feature of chronic myeloid leukemia. *Leuk Lymphoma*, *53*(8), 1569-1576. https://doi.org/10.3109/10428194.2012.656631

Tschiedel, S., Gentilini, C., Lange, T., Wolfel, C., Wolfel, T., Lennerz, V., Stevanovic, S., Rammensee, H. G., Huber, C., Cross, M., & Niederwieser, D. (2008). Identification of NM23-H2 as a tumour-associated antigen in chronic myeloid leukaemia. *Leukemia*, *22*(8), 1542-1550. https://doi.org/10.1038/leu.2008.107

Velten, L., Haas, S. F., Raffel, S., Blaszkiewicz, S., Islam, S., Hennig, B. P., Hirche, C., Lutz, C., Buss, E. C., Nowak, D., Boch, T., Hofmann, W. K., Ho, A. D., Huber, W., Trumpp, A., Essers, M. A., & Steinmetz, L. M. (2017). Human haematopoietic stem cell lineage commitment is a continuous process. *Nat Cell Biol*, *19*(4), 271-281. https://doi.org/10.1038/ncb3493

Wagner, D. E., & Klein, A. M. (2020). Lineage tracing meets single-cell omics: opportunities and challenges. *Nat Rev Genet*, *21*(7), 410-427. https://doi.org/10.1038/s41576-020-0223-2

Warfvinge, R., Geironson, L., Sommarin, M. N. E., Lang, S., Karlsson, C., Roschupkina, T., Stenke, L., Stentoft, J., Olsson-Stromberg, U., Hjorth-Hansen, H., Mustjoki, S., Soneji, S., Richter, J., & Karlsson, G. (2017). Single-cell molecular analysis defines therapy response and immunophenotype of stem cell subpopulations in CML. *Blood*, *129*(17), 2384-2394. https://doi.org/10.1182/blood-2016-07-728873

Yadav, V. K., Thakur, R. K., Eckloff, B., Baral, A., Singh, A., Halder, R., Kumar, A., Alam, M. P., Kundu, T. K., Pandita, R., Pandita, T. K., Wieben, E. D., & Chowdhury, S. (2014). Promoter-proximal transcription factor binding is transcriptionally active when coupled with nucleosome repositioning in immediate vicinity. *Nucleic Acids Res*, *42*(15), 9602-9611. https://doi.org/10.1093/nar/gku596

Yang, Z., Shah, K., Khodadadi-Jamayran, A., & Jiang, H. (2016). Dpy30 is critical for maintaining the identity and function of adult hematopoietic stem cells. *J Exp Med*, *213*(11), 2349-2364. https://doi.org/10.1084/jem.20160185

Zafar, S. Y. (2016). Financial Toxicity of Cancer Care: It's Time to Intervene. *J Natl Cancer Inst*, *108*(5). https://doi.org/10.1093/jnci/djv370

Zeng, A. G. X., Bansal, S., Jin, L., Mitchell, A., Chen, W. C., Abbas, H. A., Chan-Seng-Yue, M., Voisin, V., van Galen, P., Tierens, A., Cheok, M., Preudhomme, C., Dombret, H., Daver, N., Futreal, P. A., Minden, M. D., Kennedy, J. A., Wang, J. C. Y., & Dick, J. E. (2022). A cellular hierarchy framework for understanding heterogeneity and predicting drug response in acute myeloid leukemia. *Nat Med*, *28*(6), 1212-1223. https://doi.org/10.1038/s41591-022-01819-x

Zhang, W., Yang, B., Weng, L., Li, J., Bai, J., Wang, T., Wang, J., Ye, J., Jing, H., Jiao, Y., Chen, X., Liu, H., & Zeng, Y. X. (2020). Single cell sequencing reveals cell populations that predict primary resistance to imatinib in chronic myeloid leukemia. *Aging (Albany NY)*, *12*(24), 25337-25355. https://doi.org/10.18632/aging.104136

Zhao, H., & Deininger, M. (2021). Eradicating residual chronic myeloid leukaemia: basic research lost in translation. *Lancet Haematol*, *8*(2), e101-e104. https://doi.org/10.1016/S2352-3026(21)00001-6

Zhao, H., & Deininger, M. W. (2020). Declaration of Bcr-Abl1 independence. *Leukemia*, *34*(11), 2827-2836. https://doi.org/10.1038/s41375-020-01037-9

Zhao, H. G., & Deininger, M. (2023). Always stressed but never exhausted: how stem cells in myeloid neoplasms avoid extinction in inflammatory conditions. *Blood*, *141*(23), 2797-2812. https://doi.org/10.1182/blood.2022017152

Zhou, H., Ge, Y., Sun, L., Ma, W., Wu, J., Zhang, X., Hu, X., Eaves, C. J., Wu, D., & Zhao, Y. (2014). Growth arrest specific 2 is up-regulated in chronic myeloid leukemia cells and required for their growth. *PLoS One*, *9*(1), e86195. https://doi.org/10.1371/journal.pone.0086195

Figure 1

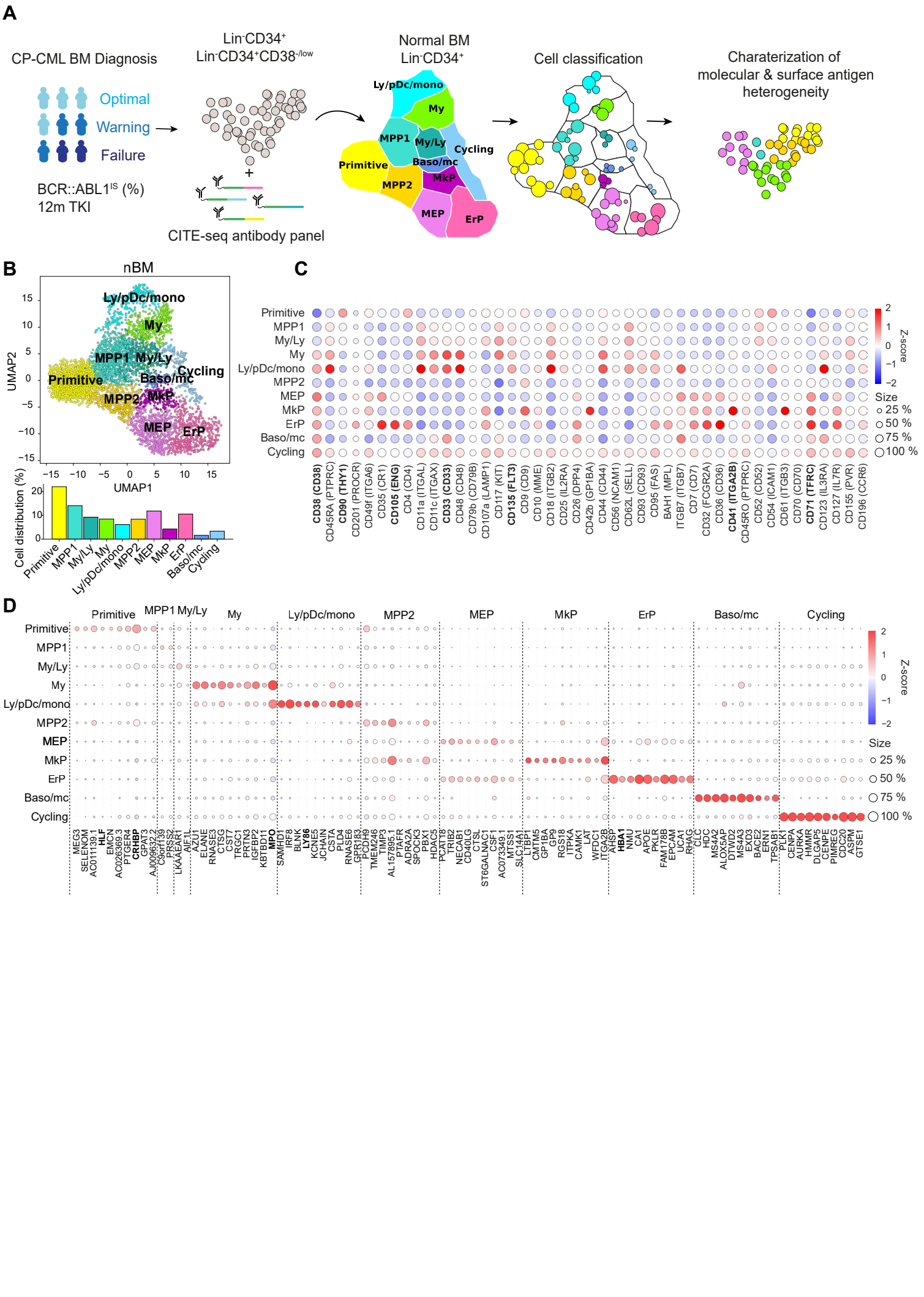

Figure 2

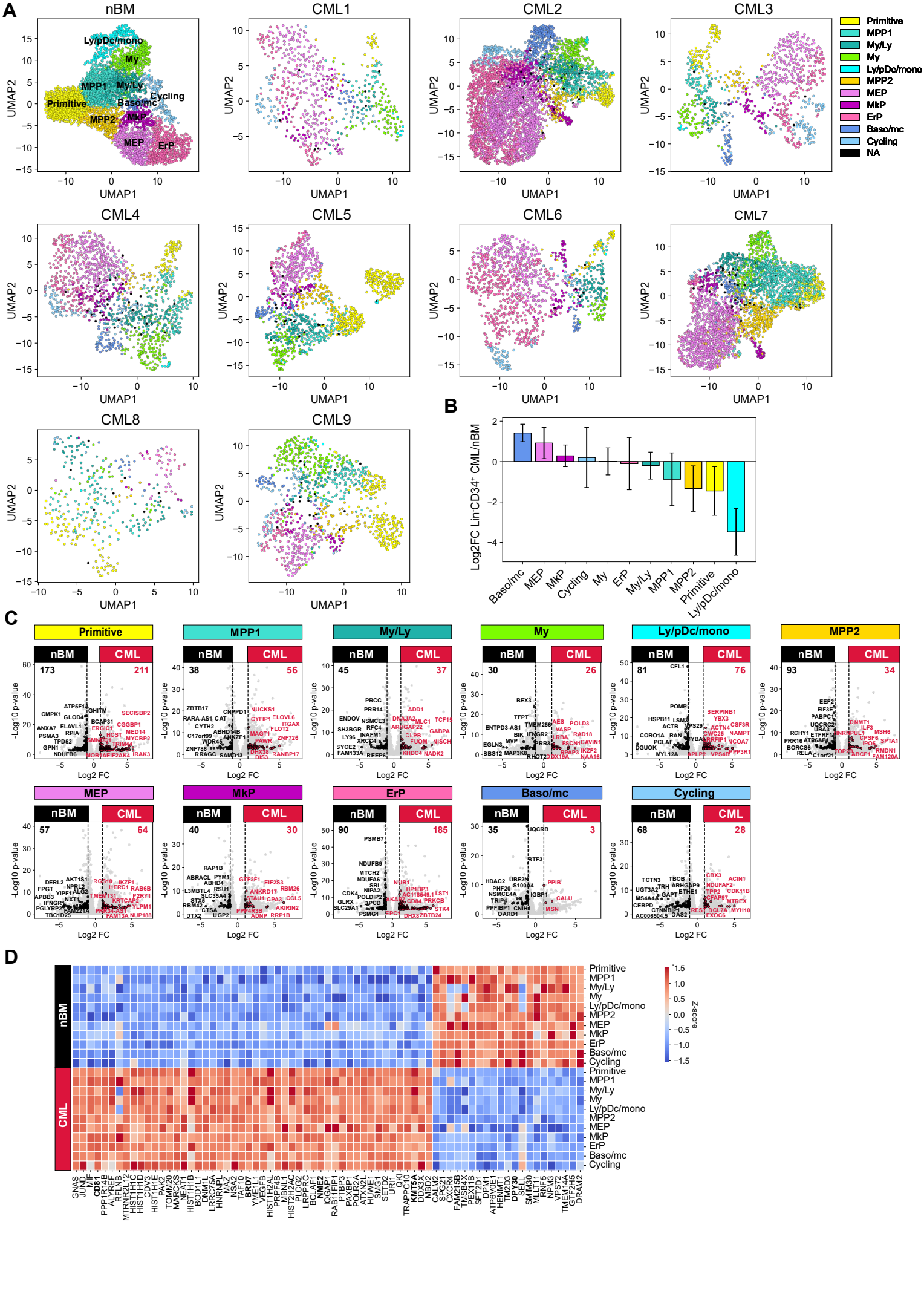

Figure 3

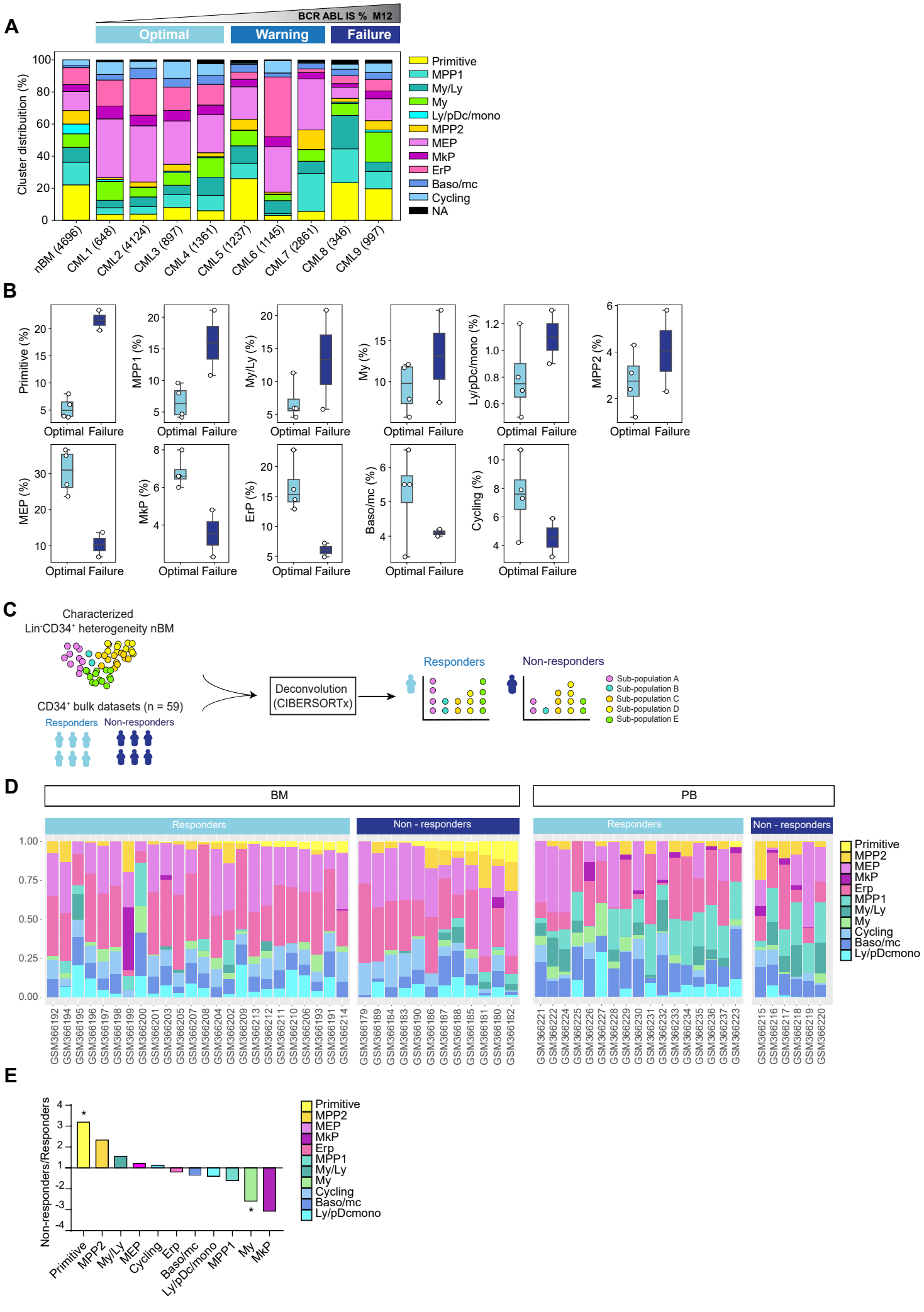

Figure 4

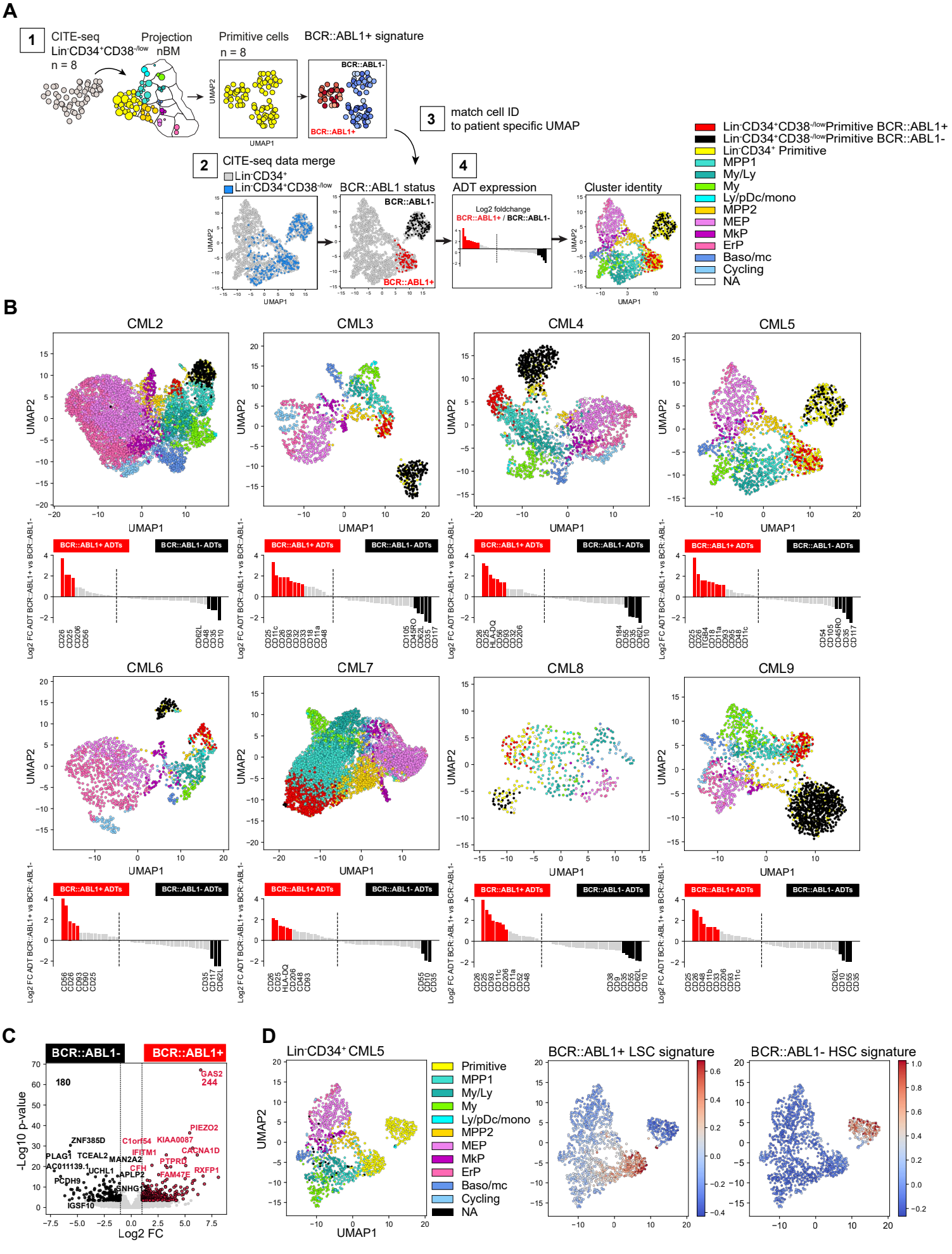

Figure 5

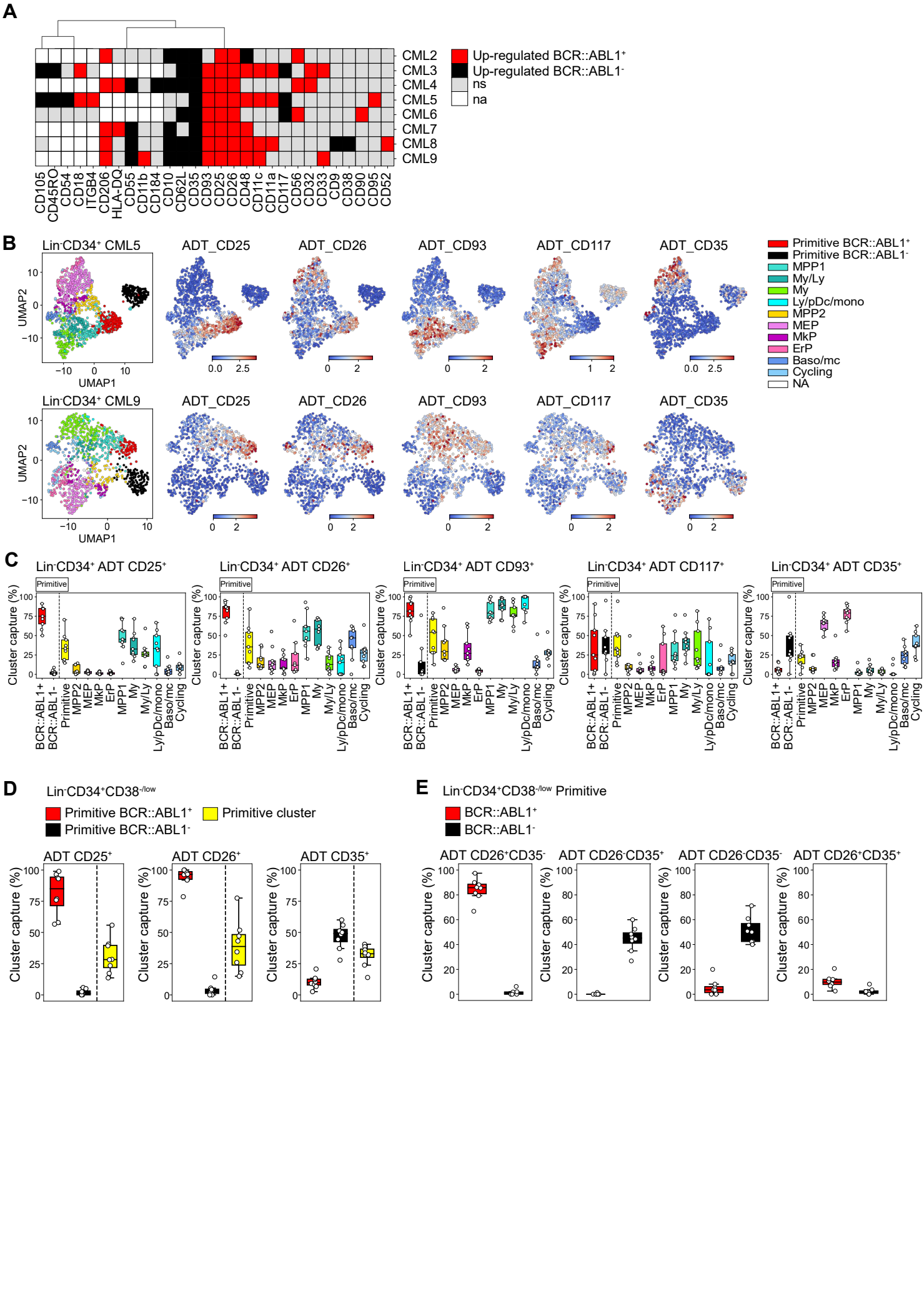

Figure 6

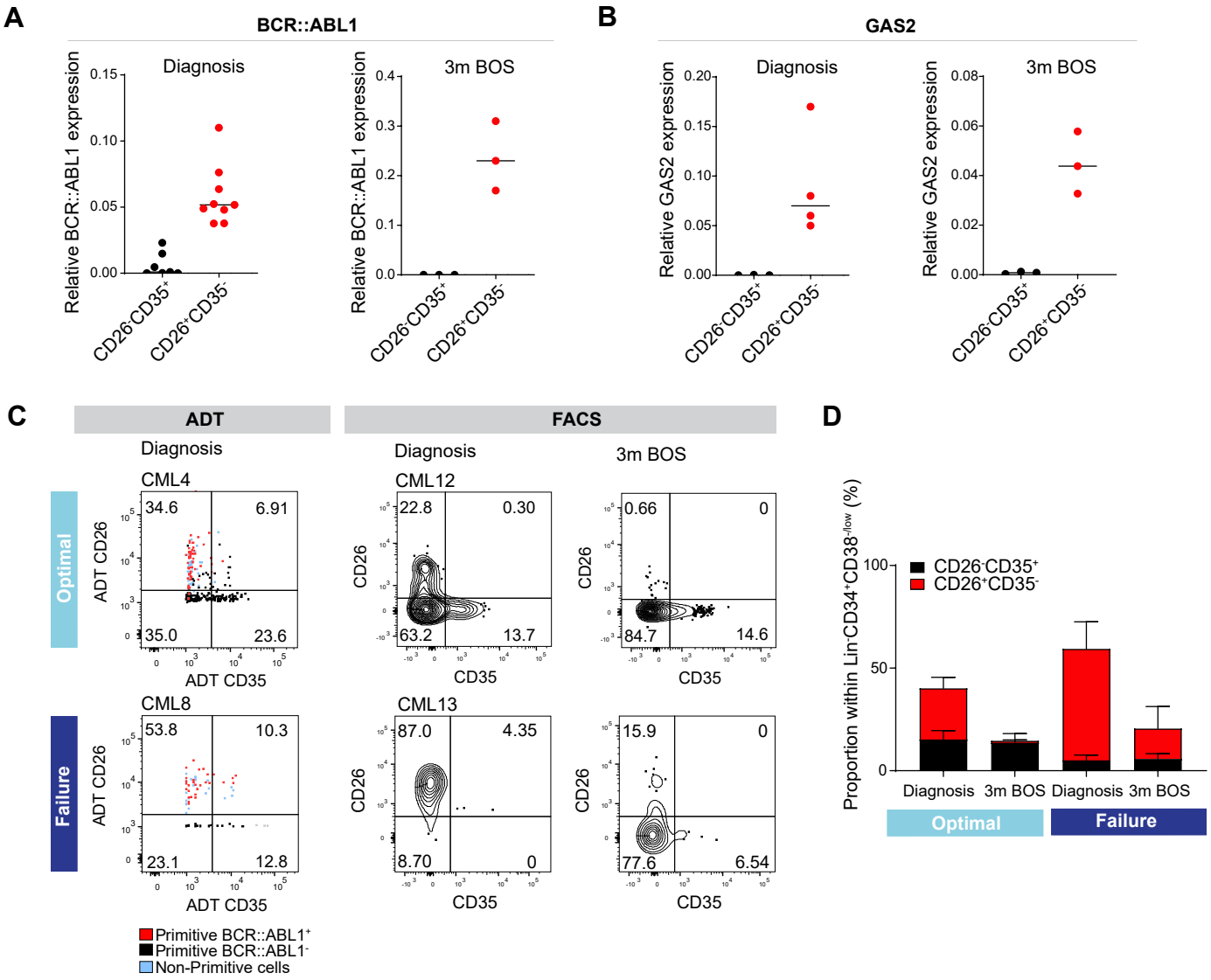

Supplementary Figure 1

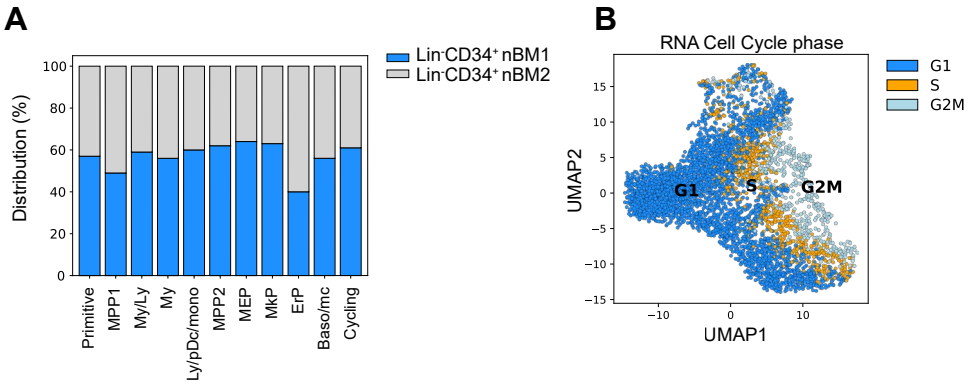

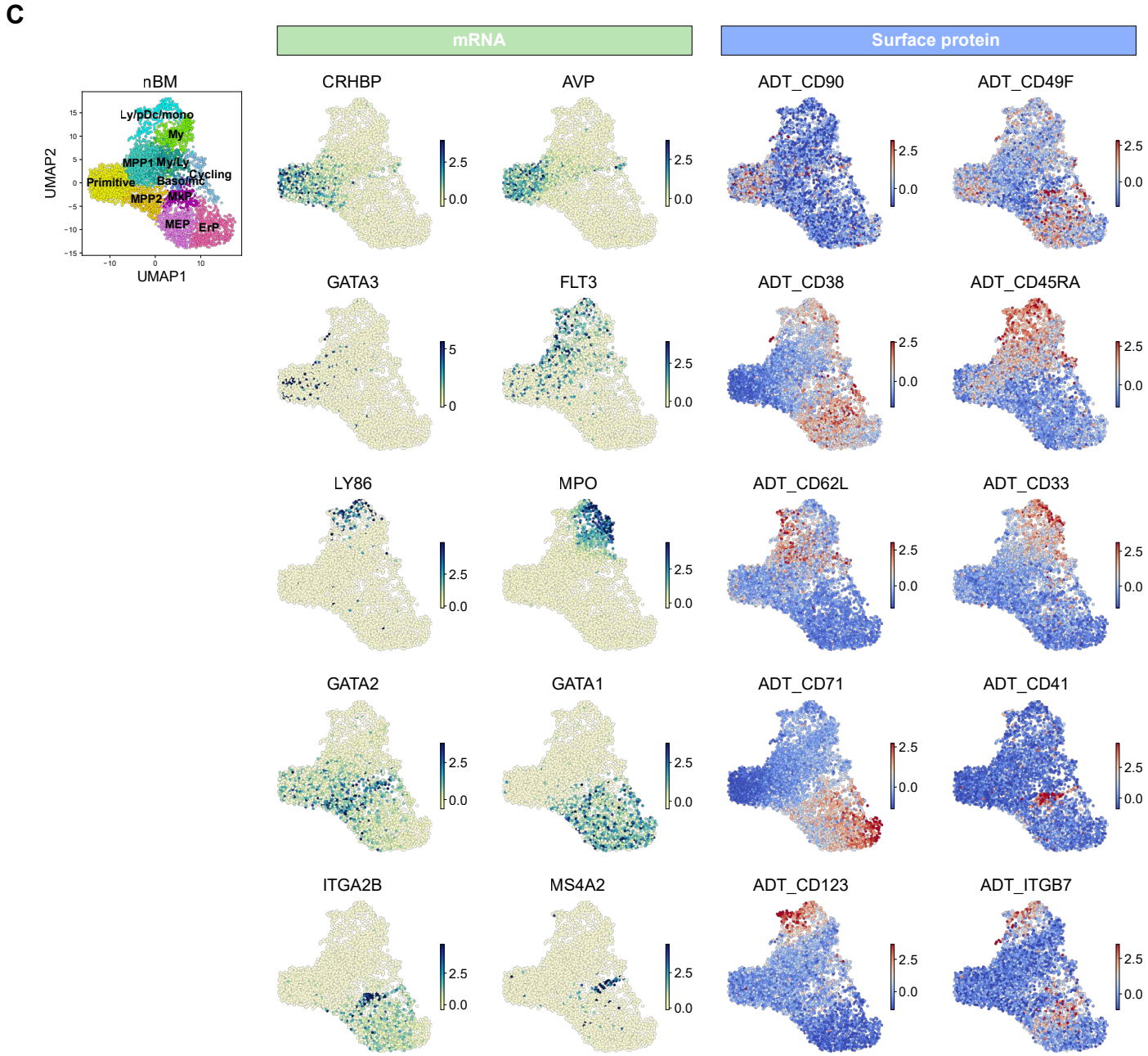

Supplementary Figure 2

A

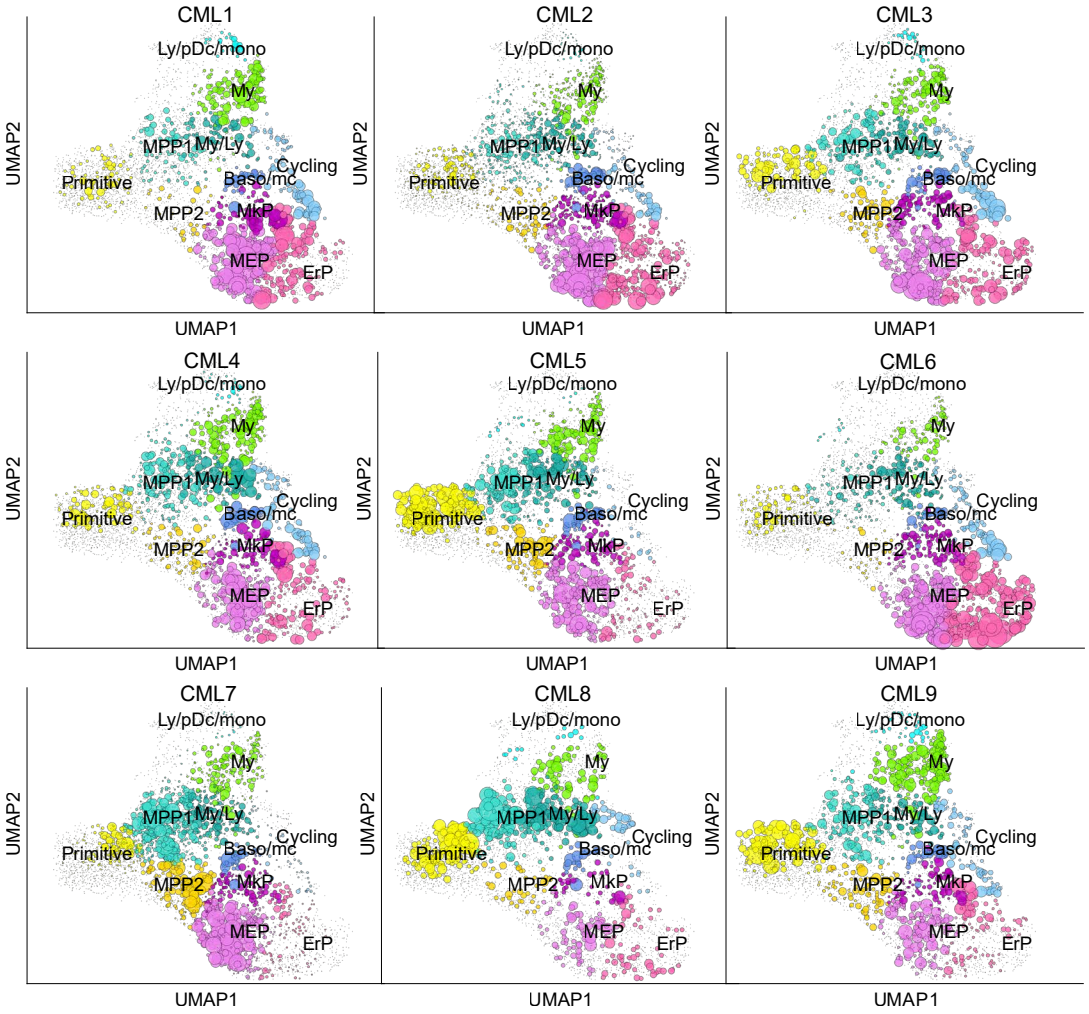

B

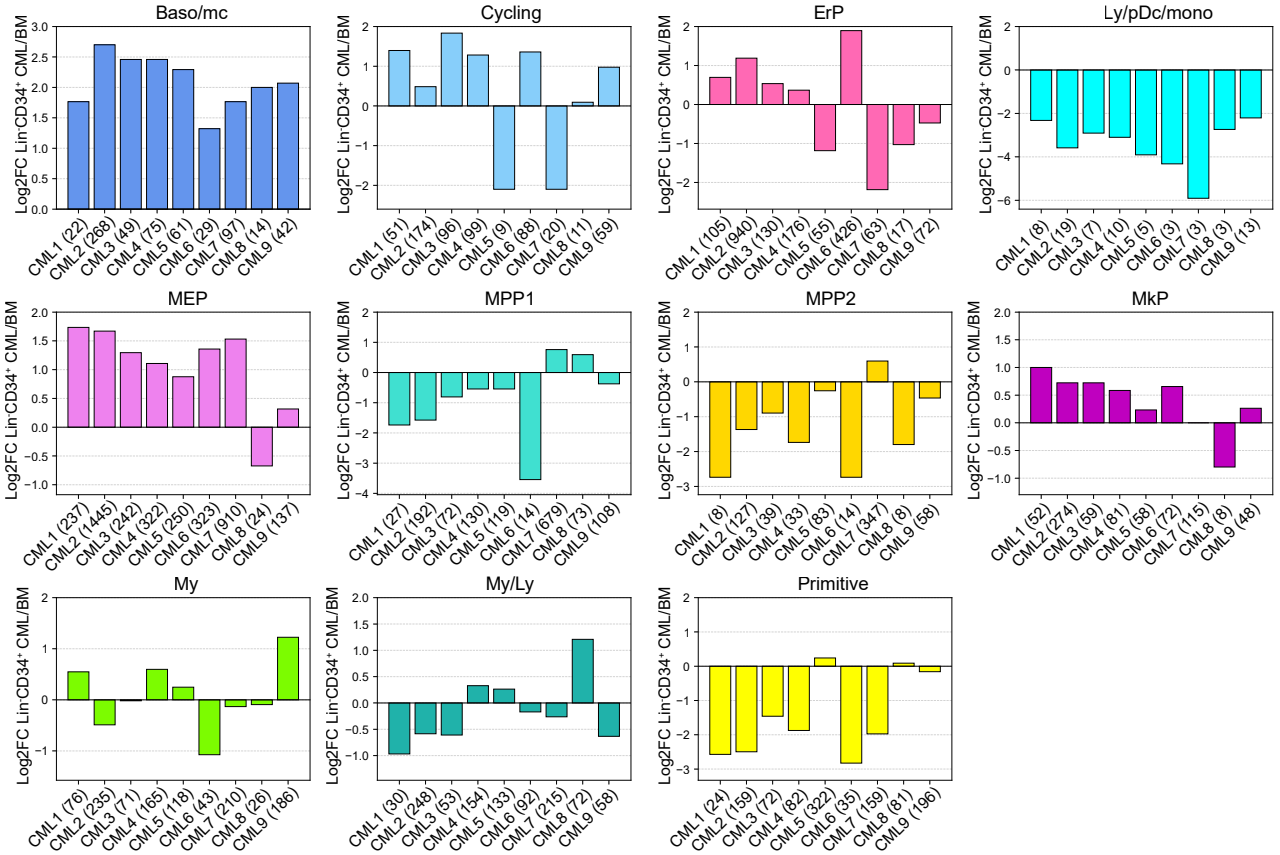

Supplementary Figure 3

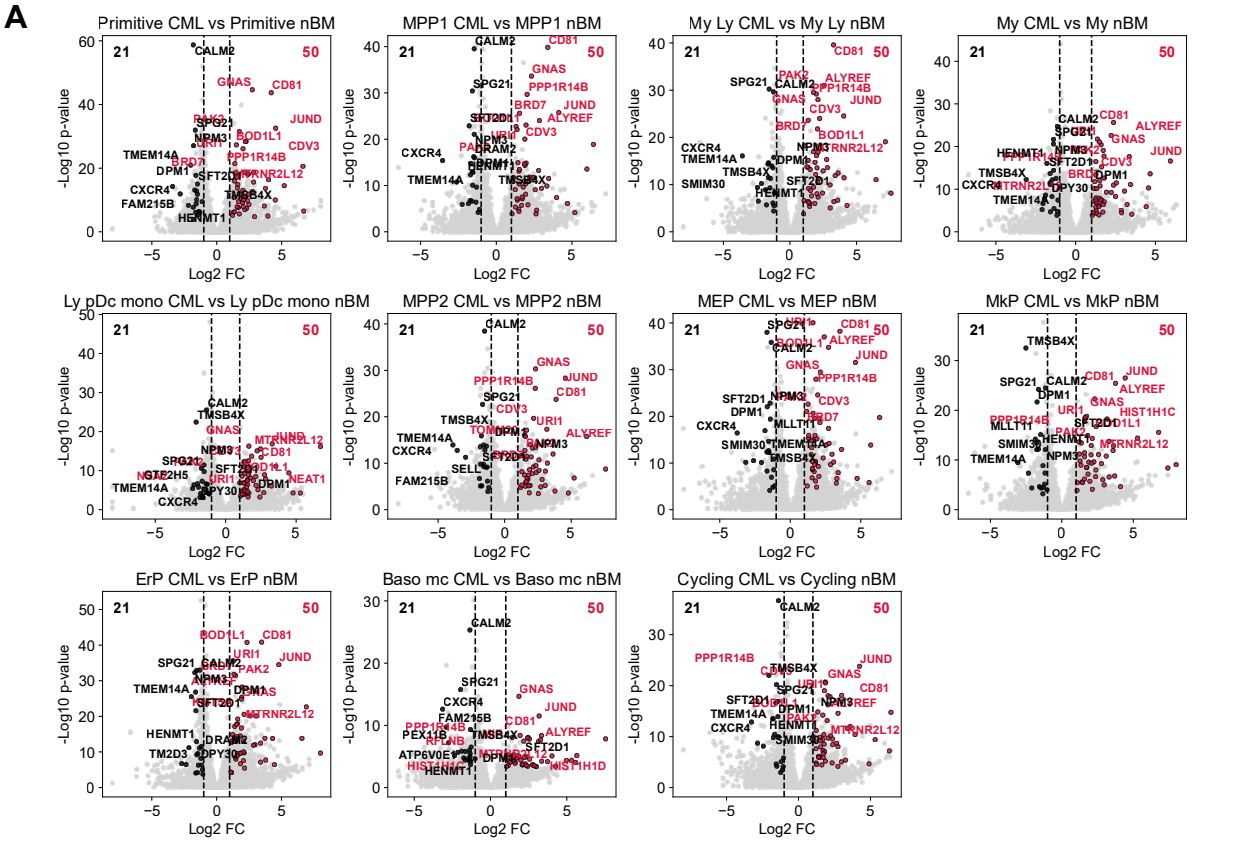

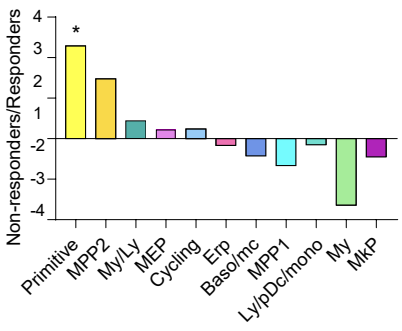

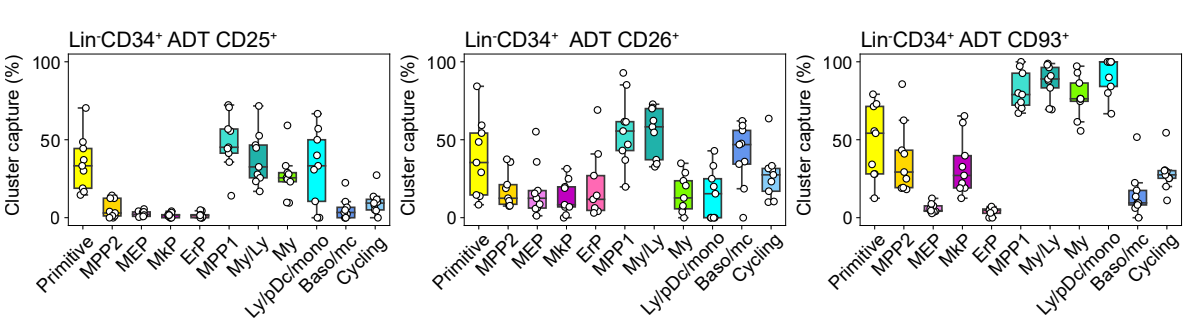

Supplementary Figure 4

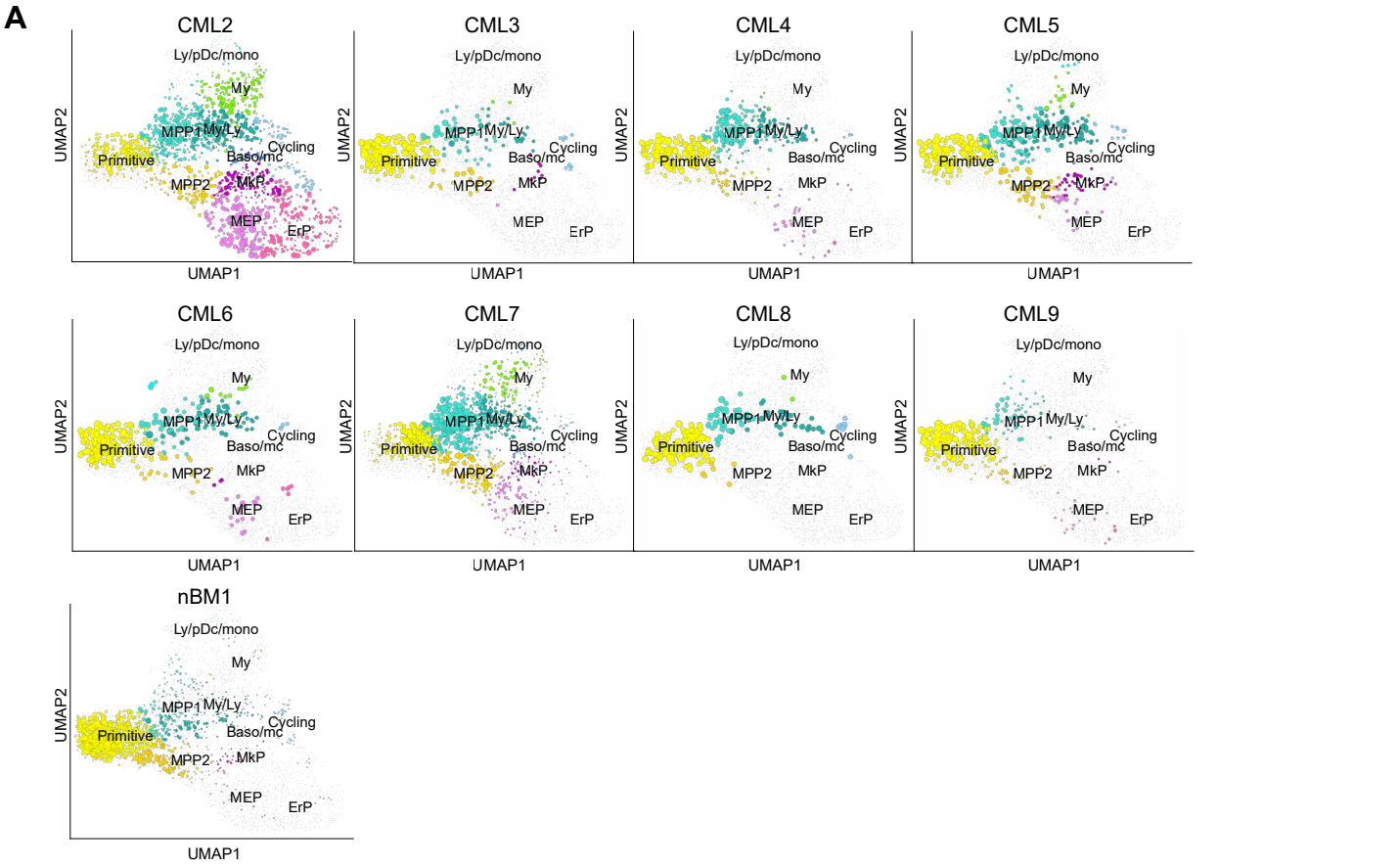

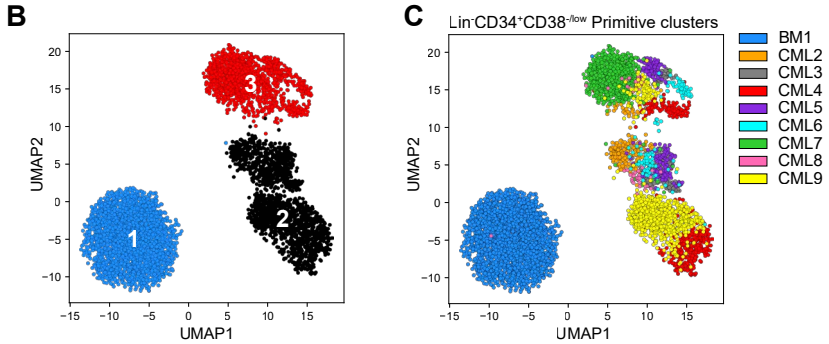

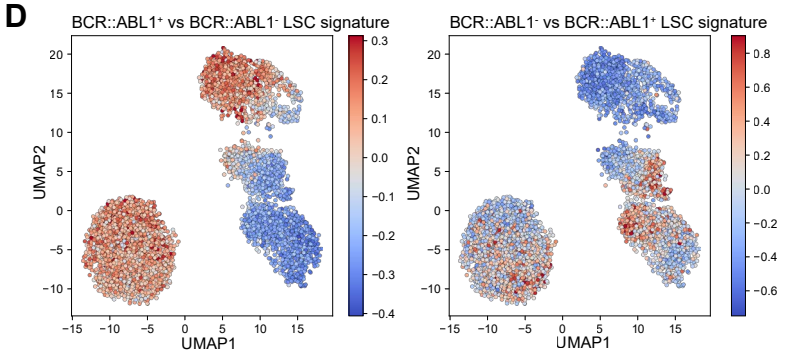

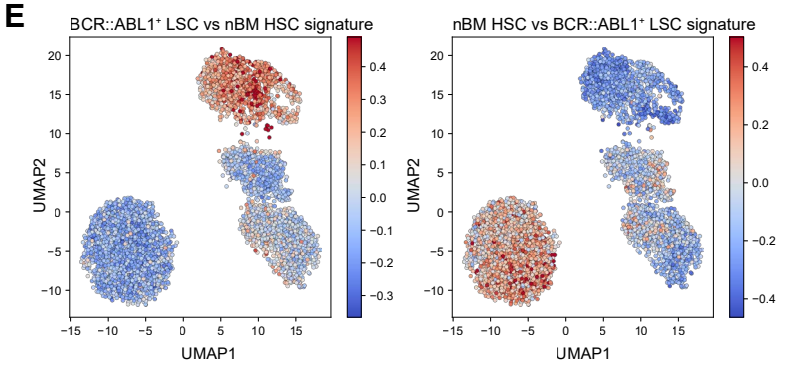

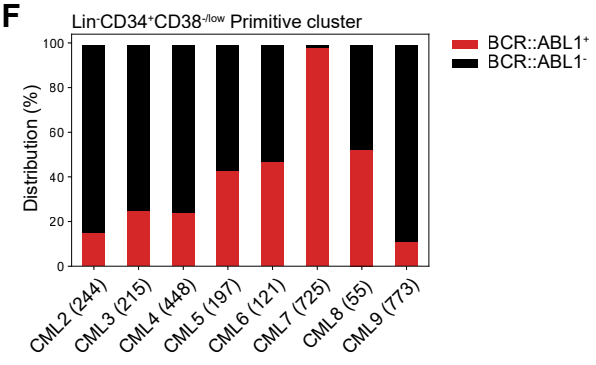

Supplementary Figure 5

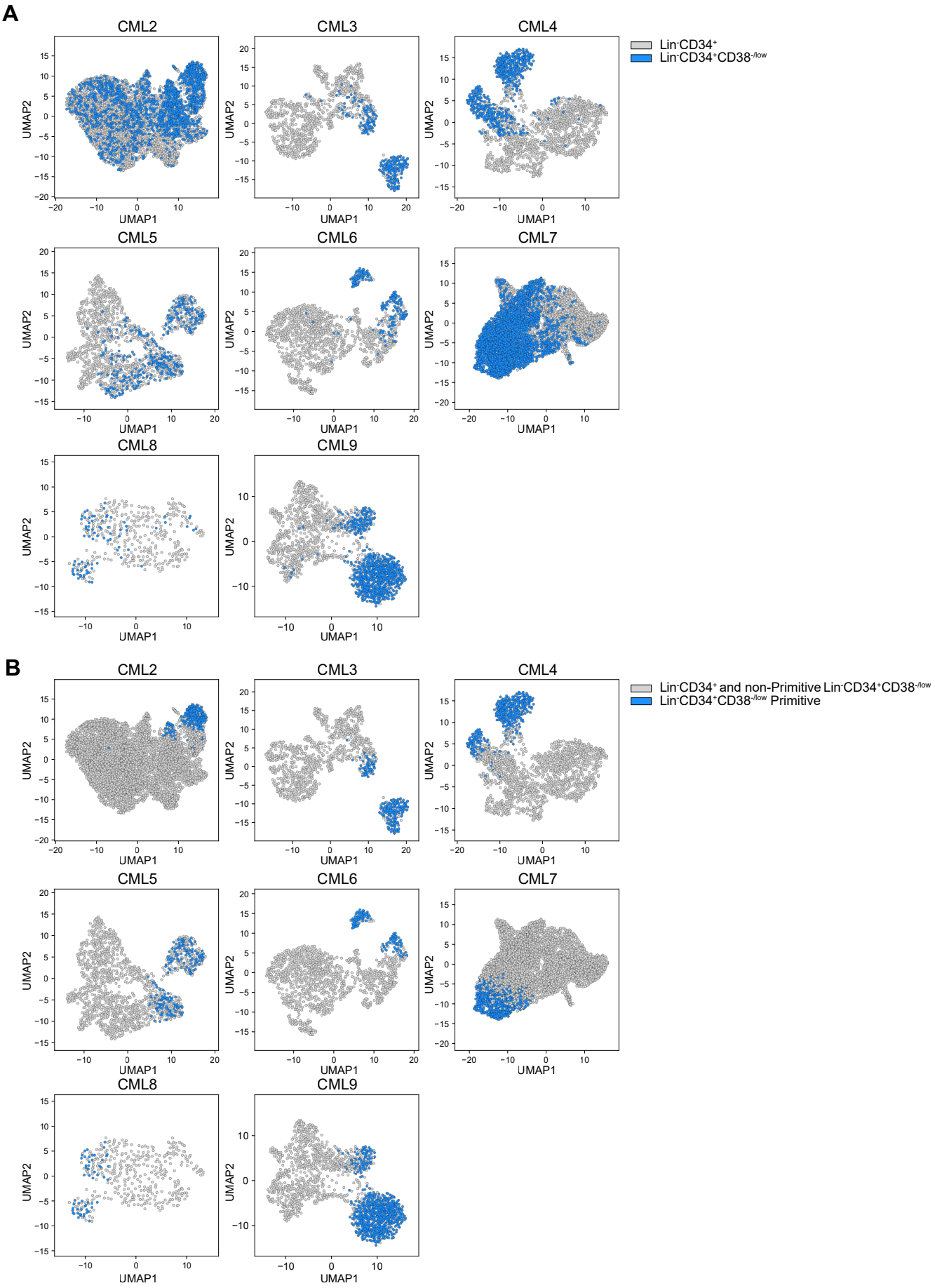

Supplementary Figure 6

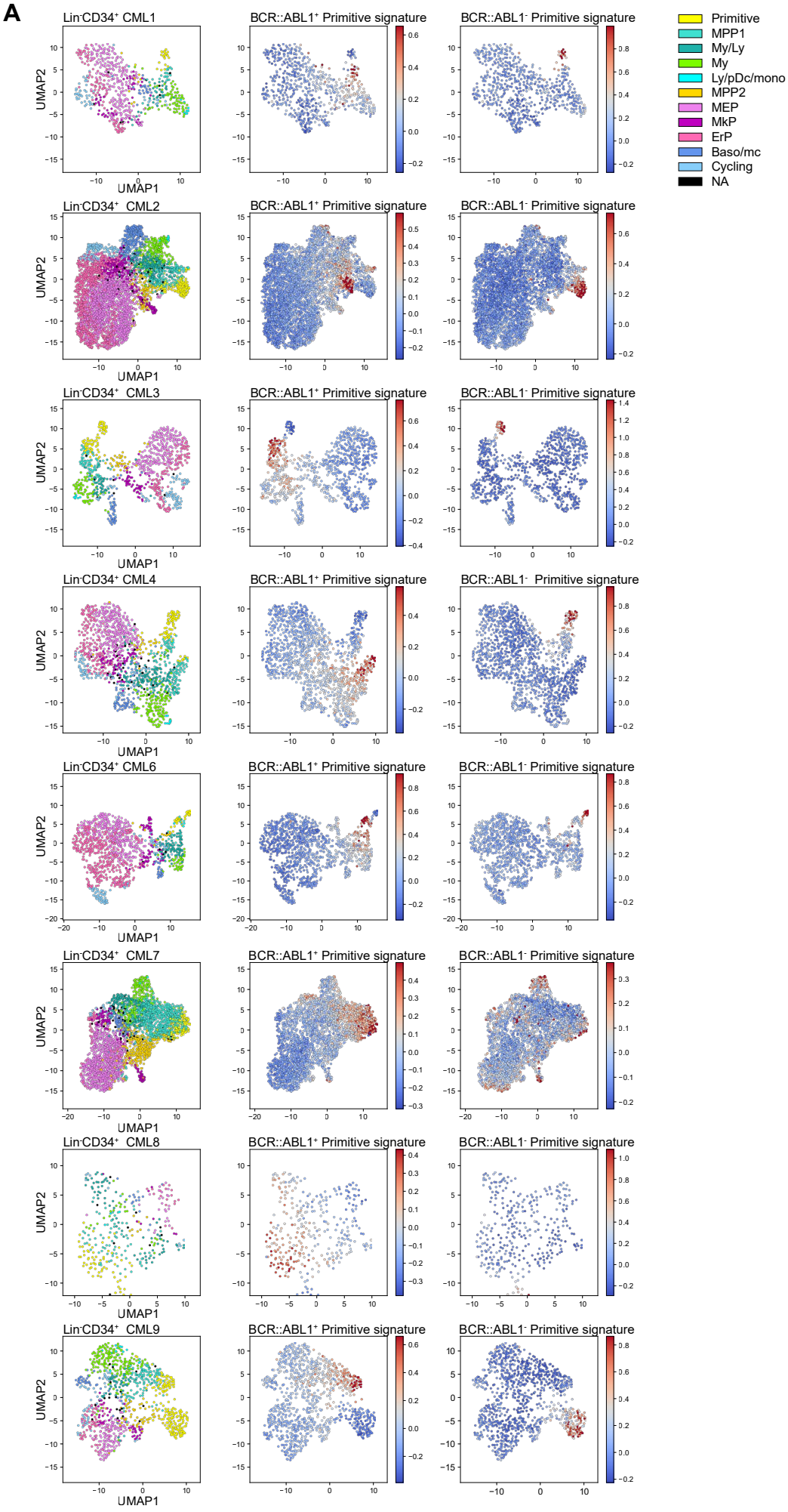

Supplementary Figure 7

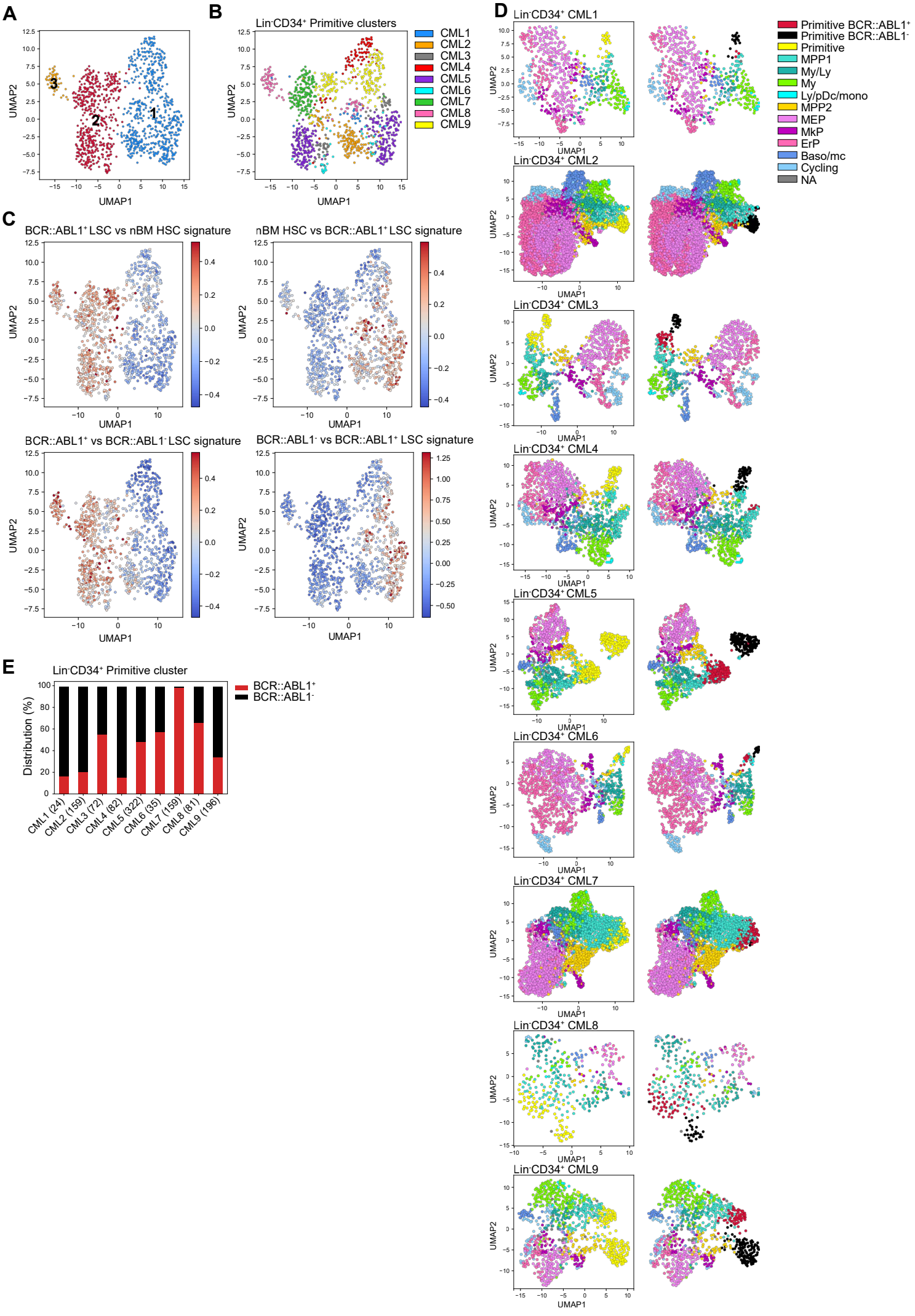

Supplementary Figure 8

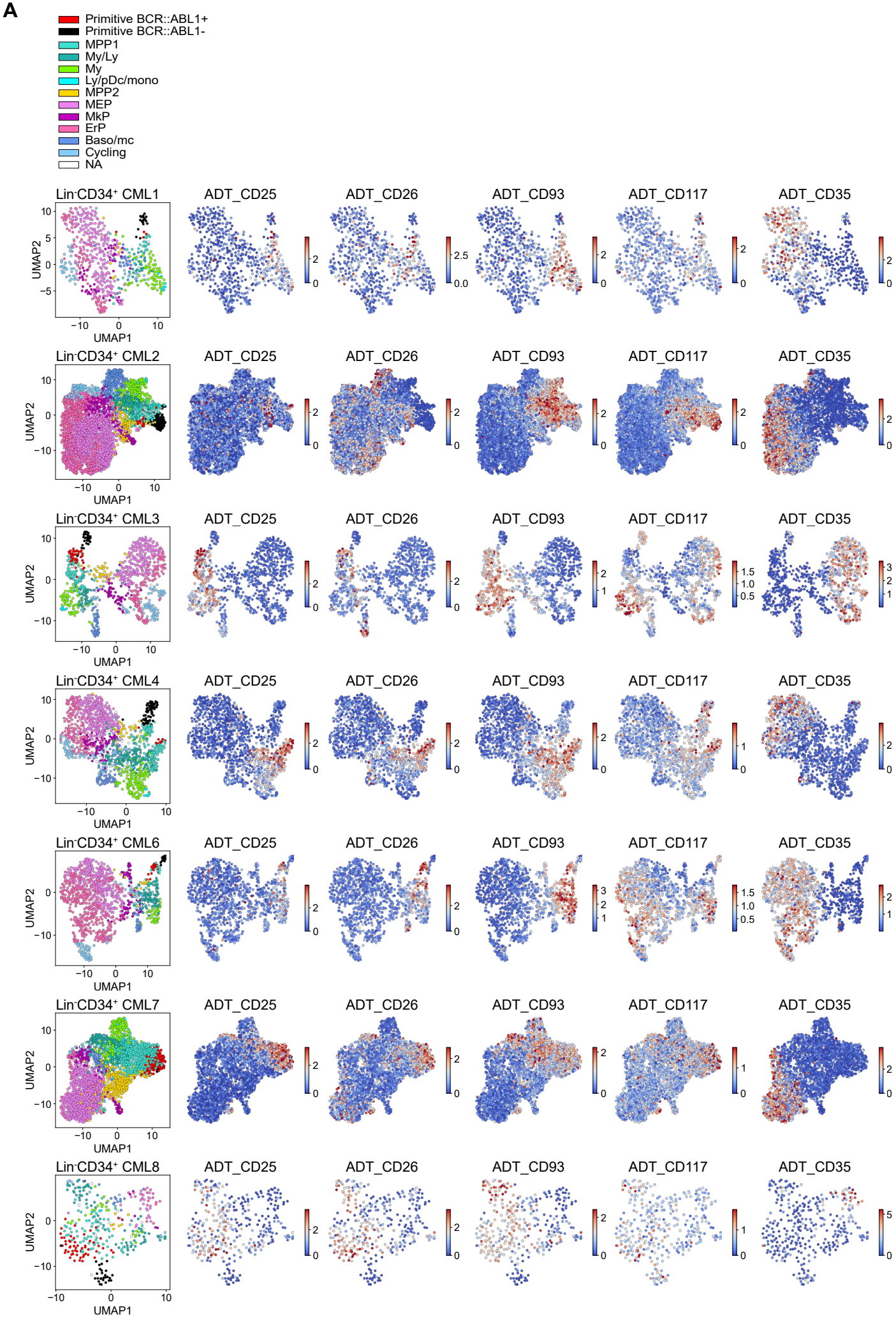

Supplementary Figure 9